

Grid-Parametrize-Split (GriPS) for Improved Scalable Inference in Spatial Big Data Analysis

Michele Peruzzi*, Sudipto Banerjee[†], David B. Dunson*, Andrew O. Finley[‡]

Abstract

Rapid advancements in spatial technologies including Geographic Information Systems (GIS) and remote sensing have generated massive amounts of spatially referenced data in a variety of scientific and data-driven industrial applications. These advancements have led to a substantial, and still expanding, literature on the modeling and analysis of spatially oriented big data. In particular, Bayesian inferences for high-dimensional spatial processes are being sought in a variety of remote-sensing applications including, but not limited to, modeling next generation Light Detection and Ranging (LiDAR) systems and other remotely sensed data. Massively scalable spatial processes, in particular Gaussian processes (GPs), are being explored extensively for the increasingly encountered big data settings. Recent developments include GPs constructed from sparse Directed Acyclic Graphs (DAGs) with a limited number of neighbors (parents) to characterize dependence across the spatial domain. The DAG can be used to devise fast algorithms for posterior sampling of the latent process, but these may exhibit pathological behavior in estimating covariance parameters. While these issues are mitigated by considering marginalized samplers that exploit the underlying sparse precision matrix, these algorithms are slower, less flexible, and oblivious of structure in the data. The current article introduces the Grid-Parametrize-Split (GriPS) approach for conducting Bayesian inference in spatially oriented big data settings by a combination of careful model construction and algorithm design to effectuate substantial improvements in MCMC convergence. We demonstrate the effectiveness of our proposed methods through simulation experiments and subsequently undertake the modeling of LiDAR outcomes and production of their predictive maps using G-LiHT and other remotely sensed variables.

Keywords: Big data; Bayesian modeling; directed acyclic graphs; Gaussian processes; sparse modeling.

*Department of Statistical Science, Duke University

[†]Department of Biostatistics, UCLA Fielding School of Public Health

[‡]Department of Forestry, Michigan State University

1 Introduction

Geographic Information Systems (GIS) and related technologies such as remote sensors, satellite imaging and portable devices that are capable of collecting precise positioning information have spawned much interest in the production of digitized geographic information, which, in turn, has led to the amassing of massive amounts of spatial data. Rapidly increasing availability and capabilities of remote sensing technologies and GIS have brought about substantial developments in modeling and analyzing spatial data in diverse scientific and data-driven industrial applications including, but not limited to, natural and environmental sciences; economics; climate science; ecology; forestry; and public health. With the abundance of spatial big data problems in the sciences and engineering, GIS and spatial data science will likely occupy a central place in the data revolution engulfing us.

With the scientific and technological communities embracing an era where open-access data-rich environments provide extraordinary opportunities to understand spatial and temporal complexity of processes, statisticians are increasingly encountering inferential questions that require complex and computationally challenging models. Analysts working with spatial technologies customarily seek to (i) estimate the variations and associations among several spatially referenced outputs; and (ii) predict outputs at new spatial locations. A generic paradigm for spatial models posits a joint probability law

$$[\text{data} \mid \text{process}] \times [\text{process} \mid \text{parameters}] \times [\text{parameters}] , \quad (1)$$

where each $[\cdot]$ represents a legitimate probability law. The above posits an underlying “process” that generates the data. Modeling this process in a rigorous and computationally efficient manner without sacrificing richness in inference presents several challenges. How exactly the underlying process is specified depends upon the data attributes relevant to inference. We focus on point-referenced data, where spatial locations are indexed by coordinates on a map. The “process” is modeled as a spatial random field over the domain of interest and the observations are treated as a finite realization of this random field. Endowing the finite-dimensional realizations of a random field with a probability law that is multivariate normal leads to the pervasive Gaussian process (GP).

The GP is, perhaps, the most conspicuous of process specifications and offers flexibility and richness in modeling. However, GPs incur onerous computational costs that make them

impracticable for spatial big data analysis. The primary burden stems from storage and computations involving the massive spatial covariance matrices representing the dependencies inside the data. The elements of these matrices are covariance functions, or kernels, depending on parameters that describe the process. These covariance functions are nonlinear and, depending upon the scientific hypotheses the model represents (e.g., nonstationary dependence), can be computationally burdensome. For irregularly situated spatial locations, as is common in geostatistics, these covariance matrices are typically dense and offer no exploitable structure to facilitate computations. Even for a modestly large number of points by today’s norms ($\approx 50,000+$), the computational demands are prohibitive. Yet, spatial analysts encounter data sets with locations numbering in the millions. The size of such data sets easily exceed common CPU and memory configurations, which means we need to rely upon statistical models to enable such analyses within available computing resources.

There exists a very large literature on scalable GP approximations for extending spatial and spatiotemporal inference to big data including, but not limited to, low-rank methods (Quiñonero-Candela and Rasmussen, 2005; Snelson and Ghahramani, 2007; Banerjee et al., 2008; Cressie and Johannesson, 2008), covariance tapering (Furrer et al., 2006; Kaufman et al., 2008), domain partitioning (Sang and Huang, 2012; Stein, 2014), divide-and-conquer methods based on meta-posteriors (Guhaniyogi and Banerjee, 2018), recursive partitioning and hierarchical matrices (Ambikasaran et al., 2016; Katzfuss, 2017; Huang and Sun, 2018; Geoga et al., 2020; Jurek and Katzfuss, 2020), Gaussian random Markov random fields (GMRF; Rue and Held, 2005), composite likelihood methods (Eidsvik et al., 2014), and local approximations (Gramacy and Apley, 2015). We refer the reader to Sun et al. (2011), Banerjee (2017), and Heaton et al. (2019) for in-depth reviews and comparisons of scalable geostatistical methods.

One particular approach that has been garnering much attention in spatial and spatiotemporal big data analysis stems from representing the joint probability law of a finite realization of the spatial process using a directed acyclic graph (DAG) constructed from the spatial locations as the nodes of the graph with parents of each node as spatial neighbors. Vecchia (1988) used this idea as a method to approximate the multivariate Gaussian likelihood function corresponding to a realized GP over a finite but large number of locations. Datta et al. (2016a) extends such finite-dimensional approximations to a well-defined spatial

process, the Nearest-Neighbor Gaussian Process (NNGP), over continuous spatial domains by defining a set of *reference* locations over which the DAG is constructed. The conditional independence of the outputs given neighboring outputs that is imposed by the DAG yields a sparse precision (inverse of covariance) matrix resulting in a sparse likelihood approximation to the full GP likelihood (often called Vecchia’s approximation in the spatial literature).

Alternative methods to build the DAG have been considered (Quiroz et al., 2019; Katzfuss and Guinness, 2019). Recently, Peruzzi et al. (2020) introduced a class of meshed Gaussian processes (MGPs) for massive spatial data sets. MGPs are constructed by mapping the nodes of a pre-determined directed acyclic graph (DAG) to groups of spatial locations. Scalability to big data follows from special choices of DAGs; treed DAGs for multivariate outcomes can be associated to recursive domain partitioning (Peruzzi and Dunson, 2020), whereas DAGs with repeated patterns arise from domain tiling or axis-parallel tessellations. In the latter case, Peruzzi et al. (2020) show that additional computational speedups correspond to data on partly observed lattices when sampling the latent process a posteriori.

However, inefficiencies associated with excessive data augmentation may arise when the data are not regularly spaced. Bayesian inference about the latent process and the parameters governing it can be carried out by collecting dependent samples from their joint posterior distribution using Markov chain Monte Carlo (MCMC) methods. Features of the posterior distribution for the parameters of interest (e.g. their mean) are estimated using such dependent samples. Efficiency of MCMC depends on (i) the computational complexity (in terms of flops and time) of the algorithm used to generate a sample of size T , and (ii) the effective sample size (ESS) of such a sample. The ESS (which is typically $T^* < T$) is the size of an i.i.d. sample from the posterior distribution with the same variance as the sample from the Markov chain. Let $\{\theta_1, \dots, \theta_T\}$ be the posterior samples of a parameter θ obtained upon convergence of an MCMC algorithm. Then, ESS is found as $T^* = T/\kappa(\theta)$, where $\kappa(\theta)$ is the autocorrelation time associated to the sequence θ_t , $t = 1, \dots, T$. Therefore, ESS measures the loss in efficiency due to the use of a Markov chain (Robert and Casella, 2005). A slowly mixing Markov chain, which exhibits high autocorrelations between successive samples, is linked to a lower ESS. Markov chains that mix poorly require substantially longer time to produce Monte Carlo samples that accurately characterize the posterior distribution. Unfortunately, mixing time increases with the dimension of the state space (see e.g. Dunson and

Johndrow, 2020), which is particularly troubling in big data settings.

Poor mixing of MCMC in spatial contexts negatively impacts the quality of estimations and uncertainty quantification of the unknown covariance parameters when sampling the high-dimensional latent process. Marginalized or collapsed samplers exhibit considerable improvements in mixing because they obviate sampling the high-dimensional spatial effects, which are subsequently sampled *after* the posterior samples of the collapsed model have been obtained. Collapsed samplers are, however, effective only for Gaussian likelihoods and tend to be much slower as they entail more expensive matrix computations (Finley et al., 2019). Furthermore, the practical performance of these algorithms in quantifying posterior uncertainty about the covariance parameters may still be unsatisfactory. Improvements compared to (faster) non-marginalized samplers may be small. Coupled with the observation that ESS is frequently much higher for the latent process than it is for covariance parameters when considering unmarginalized samplers, one may attribute poor mixing to the absence of consistent estimators for the parameters in the spatial covariance function. This has been studied for the Matérn covariance kernel for in-fill or fixed-domain spatial asymptotics (Stein, 1990; Ying, 1991; Zhang, 2004), including in models with the nugget (Tang et al., 2020). In the Bayesian context, inconsistent estimation implies that the effect of the prior does not diminish even as we increase our sample size by populating the fixed spatial domain with locations. It is also well known that model parametrizations can impact performance of MCMC (Gelfand et al., 1995; Liu and Wu, 1999; van Dyk and Meng, 2001; Yu and Meng, 2011; Kastner, 2014). The connections between parametrizations and efficiency in spatial big data contexts have not been analyzed, but we expect them to play an important role. For example, a linear model of coregionalization (LMC; Matheron, 1982; Wackernagel, 2003) for modeling multivariate spatial dependence in a Bayesian regression model (see e.g. Zhang and Banerjee, 2020) is typically associated with a “noncentered” parametrization (Papaspiliopoulos et al., 2007) that inhibits posterior sampling efficiency in scenarios that are common in geostatistical settings, e.g. when the measurement error variance is small relative to the process variance, but is otherwise computationally convenient.

In this article, we combine three separate ideas to resolve the aforementioned issues. First, we enforce a gridded (*Gri*) reference set on an MGP model to ensure sizable scalability improvements for non-gridded multivariate outcomes that may be misaligned. Second, we

parametrize (P) the LMC via Matérn covariances targeting explicit posterior sampling of the microergodic parameter (Stein, 1999), which is well identified. Third, we overparametrize the process covariance via a parameter splitting (S) strategy related to half-t priors (Gelman, 2006). The latter two ideas are based on known results but, to the best of our knowledge, their impact on multivariate spatial regression models has not been considered. In the Matérn model, P and S imply that the sill σ^2 , range $1/\phi$, and smoothness ν all have mixed centering. We then demonstrate that the combination of Grid, Parametrize, and Split, leading to a GriPS regression, results in substantial improvements in efficiency even when sampling very high-dimensional latent effects.

Our proposed methodology and related software advancements are aimed for broad application in global-scale public and private land surface monitoring efforts that rely on next generation Light Detection and Ranging (LiDAR) systems and other remotely sensed data. LiDAR provides high-dimensional characterization of land surface structures at point-referenced locations, e.g., topography, vegetation, ice/snow. Repeat measurement from these systems, and coupling with other remotely sensed data, facilitate change detection and change attribution, e.g., natural and human induced disturbances. Next generation LiDAR systems include the National Science Foundation’s National Ecological Observatory Network (NEON) Airborne Observation Platform (Kampe et al., 2010), National Aeronautics and Space Administration (NASA) ICESAT-2 (ICESat-2, 2020), Global Ecosystem Dynamics Investigation (GEDI; GEDI 2020), and Goddard LiDAR, Hyper-Spectral, and Thermal imager (G-LiHT, Cook et al. 2013). The GEDI mission sensor, mounted on the International Space Station (ISS), began collecting data in 2019 and, like ICESAT-2 and G-LiHT, is key to global-scale mapping of forest change and quantifying forest loss contribution to atmospheric CO₂ concentrations. Unlike traditional LiDAR data collection campaigns that exhaustively sample small regions, next generation LiDAR systems such as ICESAT-2, G-LiHT, and GEDI cover large spatial extents by sparsely sampling locations across the domain. While generating complete-coverage high resolution maps of forest outcomes is still of interest, there is also interest in creating predictive maps of the high-dimensional LiDAR signals over non-sampled locations.

The remainder of the article proceeds as follows. Section 2 provides an outline of a Bayesian multivariate spatial regression model and discusses the major bottlenecks that de-

tract from efficiency in MCMC samplers for current state-of-the-art models in big data settings. We then introduce GriPS in Section 3 to circumvent such bottlenecks. Section 4.1 outlines the posterior sampling algorithm whose efficiency is demonstrated in Sections 4.2 and 5 through simulation experiments and subsequent analysis of LiDAR outcomes and production of their predictive maps using G-LiHT and other remotely sensed variables.

2 Posterior sampling (in)efficiency in spatial regressions

2.1 Bayesian multivariate spatial regression models

Let $\mathcal{D} \subset \mathbb{R}^d$ denote our spatial domain and $\boldsymbol{\ell} \in \mathcal{D}$ be a generic spatial location. A multivariate spatial regression model describes the relationship between a vector of spatial outputs and predictors while incorporating a multivariate spatial process and white noise. Thus,

$$\mathbf{y}(\boldsymbol{\ell}) = \mathbf{X}(\boldsymbol{\ell})^\top \boldsymbol{\beta} + \mathbf{w}(\boldsymbol{\ell}) + \boldsymbol{\varepsilon}(\boldsymbol{\ell}), \quad (2)$$

where $\mathbf{y}(\boldsymbol{\ell}) = (y_1(\boldsymbol{\ell}), y_2(\boldsymbol{\ell}), \dots, y_q(\boldsymbol{\ell}))^\top$ is the $q \times 1$ vector of outcomes at location $\boldsymbol{\ell}$, $\mathbf{X}(\boldsymbol{\ell})^\top = \text{blockdiag}\{\mathbf{x}_i(\boldsymbol{\ell})^\top\}_{i=1}^q$ is a $q \times p$ matrix of spatially referenced predictors with each $\mathbf{x}_i(\boldsymbol{\ell})$ being $p_i \times 1$ vector of predictors corresponding to $y_i(\boldsymbol{\ell})$ at location $\boldsymbol{\ell}$ and $p = \sum_{i=1}^q p_i$, $\boldsymbol{\beta}$ is the $p \times 1$ vector of corresponding regression coefficients, $\mathbf{w}(\boldsymbol{\ell})$ and $\boldsymbol{\varepsilon}(\boldsymbol{\ell})$ are $q \times 1$ vectors of spatial random effects and random noise with elements $w_i(\boldsymbol{\ell})$ and $\varepsilon_i(\boldsymbol{\ell})$, respectively, for $i = 1, 2, \dots, q$ such that $\boldsymbol{\varepsilon}(\boldsymbol{\ell}) \stackrel{iid}{\sim} N(0, \mathbf{D})$ with a diagonal $\mathbf{D} = \text{diag}(\tau_1^2, \dots, \tau_q^2)$.

We model the uncountable set $\{\mathbf{w}(\boldsymbol{\ell}) : \boldsymbol{\ell} \in \mathcal{D}\}$ as a q -variate multivariate Gaussian process, denoted as $\mathbf{w}(\boldsymbol{\ell}) \sim GP(\mathbf{0}, \mathbf{C}_\theta(\cdot, \cdot))$, where $\mathbf{C}_\theta(\cdot, \cdot)$ is a $q \times q$ matrix-valued *cross-covariance* function indexed by parameters $\boldsymbol{\theta}$ such that $\mathbf{C}_\theta(\boldsymbol{\ell}, \boldsymbol{\ell}') = [\text{cov}\{w_i(\boldsymbol{\ell}), w_j(\boldsymbol{\ell}')\}]$ is the $q \times q$ matrix with (i, j) th element given by the covariance between $w_i(\boldsymbol{\ell})$ and $w_j(\boldsymbol{\ell}')$. Henceforth we suppress $\boldsymbol{\theta}$ in the cross-covariance to simplify notation. A valid cross-covariance satisfies: (i) $\mathbf{C}(\boldsymbol{\ell}, \boldsymbol{\ell}') = \mathbf{C}(\boldsymbol{\ell}', \boldsymbol{\ell})^\top$; and (ii) $\sum_{i=1}^n \sum_{j=1}^n \mathbf{z}_i^\top \mathbf{C}(\boldsymbol{\ell}_i, \boldsymbol{\ell}_j) \mathbf{z}_j > 0$ for any integer n and any finite collection of points $\{\boldsymbol{\ell}_1, \boldsymbol{\ell}_2, \dots, \boldsymbol{\ell}_n\}$ and for all $\mathbf{z}_i \in \mathbb{R}^q \setminus \{\mathbf{0}\}$ (see, e.g., [Genton and Kleiber, 2015](#)). Over any finite set $\mathcal{L} \subset \mathcal{D}$ the process has a multivariate normal distribution $\mathbf{w}_\mathcal{L} \sim N(0, \mathbf{C}_\mathcal{L})$, where $\mathbf{w}_\mathcal{L}$ is the $qn_\mathcal{L} \times 1$ column vector and $\mathbf{C}_\mathcal{L}$ is the $qn_\mathcal{L} \times qn_\mathcal{L}$ block matrix with the $q \times q$ matrix $\mathbf{C}(\boldsymbol{\ell}_i, \boldsymbol{\ell}_j)$ as its (i, j) block for $i, j = 1, \dots, n_\mathcal{L}$.

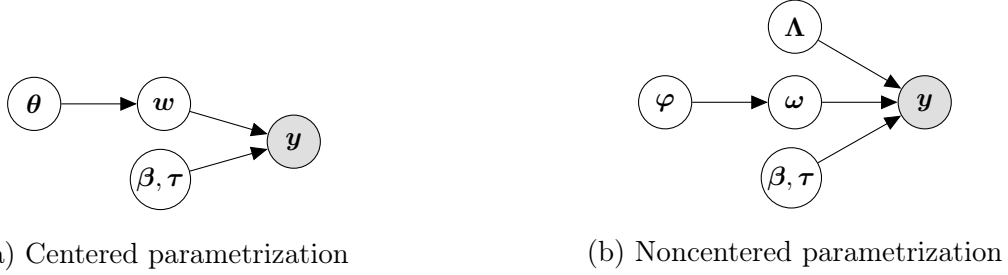


Figure 1: Common parametrizations of Bayesian spatial regression models.

Let $\mathcal{T} = \{\ell_1, \dots, \ell_n\} \subset \mathcal{D}$ be the set of locations where at least one of our q spatial outcomes has been measured. We construct $\mathbf{y}_{\mathcal{T}} = [\mathbf{y}(\ell_1)^\top, \dots, \mathbf{y}(\ell_n)^\top]^\top$ as the $nq \times 1$ vector of $\mathbf{y}(\ell_i)$'s over the n locations, analogously define $\mathbf{w}_{\mathcal{T}}$ and $\boldsymbol{\varepsilon}_{\mathcal{T}}$, and let $\mathbf{X}_{\mathcal{T}} = [\mathbf{X}(\ell_1) : \dots : \mathbf{X}(\ell_n)]^\top$. A Bayesian hierarchical model is constructed from the above specifications as

$$p(\boldsymbol{\beta}, \mathbf{w}_{\mathcal{T}}, \boldsymbol{\tau}, \boldsymbol{\theta} \mid \mathbf{y}_{\mathcal{T}}) \propto p(\boldsymbol{\tau}, \boldsymbol{\theta}) \times N(\boldsymbol{\beta}; \mathbf{m}_{\boldsymbol{\beta}}, \mathbf{V}_{\boldsymbol{\beta}}) \times N(\mathbf{w}_{\mathcal{T}}; \mathbf{0}, \mathbf{C}_{\mathcal{T}}) \times N(\mathbf{y}_{\mathcal{T}}; \mathbf{X}_{\mathcal{T}}\boldsymbol{\beta} + \mathbf{w}, \mathbf{D}_n), \quad (3)$$

where $\boldsymbol{\tau} = \{\tau_1^2, \dots, \tau_q^2\}$ and $\mathbf{D}_n = \text{blockdiag}(\{\mathbf{D}\}_{i=1}^n)$. The likelihood in (3) corresponds to $\mathbf{y} = \mathbf{X}\boldsymbol{\beta} + \mathbf{w} + \boldsymbol{\varepsilon}$, where the specification over \mathcal{T} is implicit.

Bayesian inference proceeds by sampling from the posterior distribution in (3) using MCMC algorithms. Efficiency of MCMC algorithms can be measured by effective sample size (ESS) per unit time. ESS is related to the autocorrelation in the Markov chains and measures the size of an equivalent i.i.d. sample, i.e., producing the same Monte Carlo error in ergodic averages, to the dependent MCMC samples (Liu and Chen, 1995; Robert and Casella, 2005). Scalable models effectively reduce the time for each MCMC iteration, but issues adversely affecting efficient sampling persist. We consider, in particular, the efficient inference for the cross-covariance parameters $\boldsymbol{\theta}$ and the measurement error variances $\boldsymbol{\tau}$.

2.2 Parametric specifications for multivariate spatial processes

Modeling the latent q -variate process $\mathbf{w}(\cdot)$ in (2) requires specifying a valid cross-covariance function. We consider a linear model of coregionalization (LMC),

$$\mathbf{w}(\boldsymbol{\ell}) = \sum_{j=1}^k \boldsymbol{\lambda}_j \omega_j(\boldsymbol{\ell}) = \boldsymbol{\Lambda} \boldsymbol{\omega}(\boldsymbol{\ell}) \quad (4)$$

where $\mathbf{\Lambda} = [\boldsymbol{\lambda}_1, \dots, \boldsymbol{\lambda}_k]$ is a $q \times k$ full (column) rank matrix with (i, j) th entry λ_{ij} , and each $\omega_j(\boldsymbol{\ell})$ is a univariate spatial process with correlation function $\rho_j(\boldsymbol{\ell}, \boldsymbol{\ell}') = \rho(\boldsymbol{\ell}, \boldsymbol{\ell}'; \phi_j)$. The $k \leq q$ components of $\boldsymbol{\omega}(\boldsymbol{\ell})$ are independent of each other (hence $\text{cov}\{\omega_j(\boldsymbol{\ell}), \omega_h(\boldsymbol{\ell}')\} = 0$ whenever $h \neq j$). This implies that $\boldsymbol{\omega}(\boldsymbol{\ell})$ is a multivariate spatial process with cross-correlation $\boldsymbol{\rho}(\boldsymbol{\ell}, \boldsymbol{\ell}'; \boldsymbol{\varphi})$ indexed by $\boldsymbol{\varphi} = \{\phi_1, \dots, \phi_k\}$ and $\mathbf{C}(\boldsymbol{\ell}, \boldsymbol{\ell}'; \boldsymbol{\theta}) = \mathbf{\Lambda} \boldsymbol{\rho}(\boldsymbol{\ell}, \boldsymbol{\ell}') \mathbf{\Lambda}^\top$. Under stationarity, if $\|\boldsymbol{\ell} - \boldsymbol{\ell}'\| = 0$, then $\mathbf{C}(\mathbf{0}; \boldsymbol{\theta}) = \mathbf{\Lambda} \boldsymbol{\rho}(\mathbf{0}; \boldsymbol{\varphi}) \mathbf{\Lambda}^\top = \mathbf{\Lambda} \mathbf{\Lambda}^\top$ since $\boldsymbol{\rho}(\mathbf{0}; \boldsymbol{\varphi}) = \mathbf{I}_k$. Therefore, $\mathbf{\Lambda}$ identifies with the Cholesky factorization of $\mathbf{C}(\mathbf{0})$ and is lower-triangular with positive diagonal entries (see. e.g., [Finley et al., 2008](#); [Zhang and Banerjee, 2020](#), and references therein for Bayesian LMC models). Model (2) becomes $\mathbf{y} = \mathbf{X}\boldsymbol{\beta} + (\mathbf{I}_n \otimes \mathbf{\Lambda})\boldsymbol{\omega} + \boldsymbol{\varepsilon}$. Integrating out $\boldsymbol{w} = (\mathbf{I}_n \otimes \mathbf{\Lambda})\boldsymbol{\omega}$ from the Gaussian likelihood fetches the density $p(\mathbf{y} | \mathbf{X}, \boldsymbol{\beta}, \boldsymbol{\tau}, \boldsymbol{\theta}) = N(\mathbf{y}; \mathbf{X}\boldsymbol{\beta}, \mathbf{C}_\theta + \mathbf{D}_n)$, where $\mathbf{C}_\theta = (\mathbf{I}_n \otimes \mathbf{\Lambda})\boldsymbol{\rho}_\varphi(\mathbf{I}_n \otimes \mathbf{\Lambda}^\top)$ and $\boldsymbol{\theta} = \{\mathbf{\Lambda}, \boldsymbol{\varphi}\}$, irrespective of whether we take \boldsymbol{w} or $\boldsymbol{\omega}$ as the latent process. Otherwise, different hierarchical model parametrizations can be considered ([Papaspiliopoulos et al., 2007](#)).

A *centered* parametrization (Figure 1a) implies that $\boldsymbol{\theta}$ and \mathbf{y} are conditionally independent given \boldsymbol{w} . A *noncentered* parametrization (Figure 1b) considers $\mathbf{\Lambda}$ and $\boldsymbol{\omega}$ independent a priori. A *fully-noncentered* parametrization can be built by writing $\boldsymbol{w} = (\mathbf{I}_n \otimes \mathbf{\Lambda})\mathbf{L}_\varphi \mathbf{u}$ where $\mathbf{L}_\varphi \mathbf{L}_\varphi^\top = \boldsymbol{\rho}_\varphi$ and \mathbf{u} is white noise—the graphical model reads $\mathbf{u} \rightarrow \mathbf{y}$ and $\boldsymbol{\theta} \rightarrow \mathbf{y}$. The difference between centered and noncentered parametrizations is best appreciated via a simple example. If $q = 1$, in the centered model we may let $\mathbf{\Lambda} = \sigma > 0$ and assign prior $\sigma^2 \sim \text{InvG}(\sigma^2; a, b)$. Then, the full conditional posterior is $p(\sigma^2 | \boldsymbol{w}, \mathbf{y}) = p(\sigma^2 | \boldsymbol{w}) = \text{InvG}(\sigma^2; a^*, b^*)$ where $a^* = a + n/2$ and $b^* = b + \frac{1}{2}\boldsymbol{w}^\top \mathbf{C}_\theta^{-1} \boldsymbol{w}$. In the noncentered models, $\mathbf{\Lambda} = \lambda > 0$ can be assigned e.g. a truncated Gaussian prior $N(\lambda; m, v)\mathbf{1}(\lambda > 0)$, resulting in a truncated Gaussian full conditional posterior, with variance $v^* = (v^{-1} + \boldsymbol{\omega}^\top \boldsymbol{\omega} / \tau^2)^{-1}$, mean $m^* = v^* \boldsymbol{\omega}^\top (\mathbf{y} - \mathbf{X}\boldsymbol{\beta}) / \tau^2$, and truncation below zero. Updating $\boldsymbol{\varphi}$ in all models typically proceeds via Metropolis steps, hence the fully noncentered model provides no additional advantage and we will not consider it further.

Specifically, we expect the relative efficiency of the noncentered models to be poor when the ratio between the noise variance and process variance is small ([Papaspiliopoulos et al., 2007](#)). As this commonly occurs in geospatial settings, the centered parametrization might lead to better MCMC performance. However, noncentered models are advantageous as they involve k a-priori independent processes rather than q dependent ones, leading to more

convenient updates for Λ , especially when setting $k < q$ as in a spatial factor model (Ren and Banerjee, 2013; Taylor-Rodriguez et al., 2019; Zhang and Banerjee, 2020).

2.3 Weak identifiability of Matérn covariance functions

The LMC of Section 2.2 requires the specification of the k correlation functions $\phi_j(\cdot, \cdot)$. The Matérn model is a parsimonious but flexible choice in this context. For a univariate spatial process $\omega(\cdot) \sim GP(0, C_\theta)$, one assumes that $\text{cov}\{\omega(\ell), \omega(\ell')\} = \sigma^2 \rho(\ell, \ell'; \{\phi, \nu\})$, where

$$\rho(\ell, \ell'; \{\phi, \nu\}) = \frac{2^{1-\nu}}{\Gamma(\nu)} \phi^\nu \|\ell - \ell'\|^\nu K_\nu(\phi \|\ell - \ell'\|), \quad (5)$$

and K_ν is the modified Bessel function of the second kind of order ν . We know that $\theta = \{\sigma^2, \phi, \nu\}$ are weakly identified (Banerjee et al., 2014). In fixed-domain asymptotics, only the microergodic parameter $\{\sigma^2 \phi^{2\nu}\}$ can be estimated consistently (Stein, 1990; Ying, 1991; Zhang, 2004; Tang et al., 2020). In practice, predictions at unknown locations are less sensitive to the individual parameters' value, since $\sigma^2 \phi^{2\nu}$ matters more for spatial interpolation. Nevertheless, weak identifiability is expected to adversely impact MCMC mixing and convergence for $\{\sigma^2, \phi, \nu\}$. If one seeks to estimate the individual parameters and quantify uncertainty, informative priors become necessary. It is not uncommon in these contexts to fix some parameters to reasonable values, constrain the prior on a grid, or perform greedy searches for optimal values through cross-validation (Shirota et al., 2019; Banerjee, 2020).

2.4 Pitfalls of marginalization

Spatial dependence of the outcomes in (2) is modeled using the latent process. Integrating out the latent effects from (3) yields the marginal or collapsed Bayesian model

$$p(\beta, \tau, \theta | \mathbf{y}) \propto p(\tau, \theta) \times N(\beta; \mu_\beta, \mathbf{V}_\beta) \times N(\mathbf{y}; \mathbf{X}\beta, \mathbf{C}_\theta + \mathbf{D}_n). \quad (6)$$

Now we can sample the unknown parameters $\{\beta, \tau, \theta\}$ from (6). This is appealing because we avoid sampling the high dimensional \mathbf{w} , a step that is known to significantly encumber MCMC mixing and convergence for parameters that are highly correlated to \mathbf{w} a posteriori. Even without \mathbf{w} in (6), we can sample from $p(\mathbf{w} | \mathbf{y})$ by drawing one \mathbf{w} from $p(\mathbf{w} | \beta, \tau, \theta, \mathbf{y})$, which is Gaussian, for each sampled value of $\{\beta, \tau, \theta\}$ from (6).

Sampling from (6), however, entails $(\mathbf{C}_\theta + \mathbf{D}_n)^{-1}$ and its determinant, which becomes prohibitive in big data settings. To further elucidate, the chief computational burden arises from the Cholesky decomposition of $\mathbf{K}_\theta = \mathbf{C}_\theta + \mathbf{D}_n$ or its inverse. Once the Cholesky decomposition has been computed, say $\text{chol}(\mathbf{K}_\theta) = \mathbf{L}\mathbf{F}\mathbf{L}^\top$, where $\mathbf{L} = [l_{ii}]$ is unit lower triangular (with $l_{ii} = 1$) and $\mathbf{F} = \text{diag}[f_{ii}]$ is diagonal with $f_{ii} > 0$, then

$$\log N(\mathbf{y}; \mathbf{X}\boldsymbol{\beta}, \mathbf{C}_\theta + \mathbf{D}_n) = \text{constant} - \frac{1}{2} \sum_{i=1}^n \log(f_{ii}) - \frac{1}{2} \sum_{i=1}^n \frac{u_i^2}{f_{ii}}, \quad (7)$$

where u_i is the i -th element of the vector \mathbf{u} that solves the lower-triangular system $\mathbf{L}\mathbf{u} = \mathbf{y} - \mathbf{X}\boldsymbol{\beta}$. Given the Cholesky decomposition, computing (7) is cheap (of $O(nq)$). However, the Cholesky decomposition itself involves $O(n^3q^3)$ floating point operations (flops) and $O(n^2q^2)$ in storage complexity and, hence, is impracticable for very large values of nq .

One option to improve computational speed is to replace $\mathbf{w}(\cdot)$ with a low-rank process $\tilde{\mathbf{w}}(\cdot)$ with covariance function $\tilde{\mathbf{C}}_\theta(\boldsymbol{\ell}, \boldsymbol{\ell}') = \mathbf{C}_\theta(\boldsymbol{\ell}, \mathcal{S})\mathbf{C}_\theta^{-1}(\mathcal{S})\mathbf{C}_\theta(\mathcal{S}, \boldsymbol{\ell}')$, where \mathcal{S} is a set of n_k knots (Banerjee et al., 2008). In this case, the Sherman-Woodbury-Morrison (SWM) identity and the matrix determinant lemma on the integrated covariance $\tilde{\mathbf{C}}_\theta + \mathbf{D}_n = \mathbf{C}_\theta(\boldsymbol{\ell}, \mathcal{S})\mathbf{C}_\theta^{-1}(\mathcal{S})\mathbf{C}_\theta(\mathcal{S}, \boldsymbol{\ell}') + \mathbf{D}_n$ imply that one only needs to compute $\mathbf{C}_\theta^{-1}(\mathcal{S})$ which is of size $n_k \times n_k$ rather than $n \times n$. Directly computing the SWM identity is not optimal and can be avoided using $\text{chol}(\mathbf{C}_\theta(\mathcal{S}))$ (see Banerjee, 2017, for details).

Greater scalability is achieved when $\mathbf{w}(\cdot)$ is replaced by any DAG-based process such as an NNGP or an MGP. Here, \mathbf{C}_θ is replaced by $\tilde{\mathbf{C}}_\theta$ such that $\tilde{\mathbf{C}}_\theta^{-1}$ is sparse. Computations will ultimately depend on $(\mathbf{C}_\theta^{-1} + \mathbf{D}_n^{-1})^{-1}$ and its determinant. This relies on sparse libraries (e.g. sparse Cholesky) which, unfortunately, can impede iterative computations in big data analysis and may be circumvented in some special circumstances (Peruzzi and Dunson, 2020). Alternatively, one can directly model the responses as a sparse GP, in which case the original cross-covariance function $\mathbf{C}_\theta(\boldsymbol{\ell}, \boldsymbol{\ell}')$ is first replaced by $\tilde{\mathbf{C}}_\theta(\boldsymbol{\ell}, \boldsymbol{\ell}') = \mathbf{C}(\boldsymbol{\ell}, \boldsymbol{\ell}')_\theta + \delta_{\boldsymbol{\ell}=\boldsymbol{\ell}'}\{\mathbf{D}\}$, then the resulting full model's precision $\tilde{\mathbf{C}}_\theta^{-1}$ is directly replaced by a sparse counterpart $\tilde{\tilde{\mathbf{C}}}_\theta^{-1}$. Now one does not need sparse Cholesky libraries as $\tilde{\tilde{\mathbf{C}}}_\theta^{-1}$ and its determinant are computed directly from the DAG Finley et al. (2019). This model does not include latent effects, but Vecchia approximations on the latent effects tend to produce inference closer to the full GP model than the response model (Katzfuss and Guinness, 2019). While marginalization avoids some issues related to model parametrization, it does not address the weak identifiability of

the Matérn parameters in (5). Finally, the marginal and response models are only feasible when all outcomes are Gaussian. Sampling \mathbf{w} a posteriori is, therefore, more generally applicable.

2.5 QMGPs at irregularly-spaced locations

Let us return to the Bayesian hierarchical model in (3) that explicitly includes \mathbf{w} . While β and \mathbf{w} can be directly updated using Gibbs steps from their (Gaussian) full conditional distributions and τ can also be updated directly if we assign independent conjugate distributions (Inverse-Gamma) for each τ_i^2 , the cross-covariance parameters θ do not render closed-form full conditional distributions. Therefore, we update θ using some stationarity-preserving MCMC method such as Metropolis random walk of Hamiltonian Monte Carlo. These entail computing, up to a proportionality constant, a density proportional to $p(\mathbf{w} | \theta) = N(\mathbf{w}; \mathbf{0}, \mathbf{C}_\theta) \times p(\theta)$, where $p(\theta)$ is any proper prior distribution for θ . Unfortunately, once again, we are faced with computing the inverse and determinant of a high-dimensional covariance matrix.

Scalable methods accrue significant benefits in computing $p(\mathbf{w} | \theta)$. In particular, a “cubic” meshed GP (QMGP; Peruzzi et al., 2020) produces a reversal in the balance of computational costs: evaluations of $p(\mathbf{w} | \theta)$ become faster than sampling \mathbf{w} —usually they are about 10 times slower. In order to achieve such speedups, one requires that the so-called *reference* set \mathcal{S} be defined on a regular grid. \mathcal{S} is akin to the set of “knots” or “sensors” in low rank methods, whose choice is not a trivial matter, see e.g. Krause et al. (2008) or Guhaniyogi et al. (2011). Standard QMGPs are associated with MCMC efficiency losses when a gridded reference set does not overlap with the measurement locations. In this case the size of the latent effects might greatly exceed the sample size, with negative impacts on MCMC mixing and convergence of the centered parameters. We clarify this point after building the QMGP that we subsequently use in the remainder of the article.

For any given finite set \mathcal{L} of spatial locations and a fixed reference set \mathcal{S} , let $\mathcal{U} = \mathcal{L} \setminus \mathcal{S}$ denote the *non-reference* locations. We partition the domain using an axis-parallel tessellation $\mathbf{T} = \{D_j\}_{j=1}^M$ such that $\mathcal{D} = \cup_{j=1}^M D_j$, where $M = \prod_{i=1}^d M_i$. We then partition the reference and non-reference sets into $\mathcal{S} = \cup_{i=1}^M S_i$ and $\mathcal{U} = \cup_{i=1}^M U_i$, where $S_i = \mathcal{S} \cap D_i$ and $U_i = \mathcal{U} \cap D_i$. Let the DAG $\mathcal{G} = \{\mathbf{V}, \mathbf{E}\}$ have nodes $\mathbf{V} = \mathbf{A} \cup \mathbf{B}$ where \mathbf{A} and

\mathbf{B} are the $2M$ reference and non-reference nodes, respectively. \mathcal{T} and \mathcal{G} are linked via $\eta : \mathcal{D} \rightarrow \mathbf{V}$ which maps any reference location to a node in \mathbf{A} and any non-reference location to a node in \mathbf{B} . The parent set of nodes for $\mathbf{v} \in \mathbf{V}$ is denoted as $\text{Pa}[\mathbf{v}]$, and $\mathbf{E} = \{\text{Pa}[\mathbf{v}]\}_{\mathbf{v} \in \mathbf{V}}$. By construction, we let $\text{Pa}[\mathbf{v}] \subset \mathbf{A}$ if $\mathbf{v} \in \mathbf{B}$, i.e. non-reference nodes have no children. Furthermore, in the cubic MGP’s specification of \mathcal{G} we have $|\text{Pa}[\mathbf{v}]| \leq d$ and $|\text{Ch}[\mathbf{v}] \cap \mathbf{A}| \leq d$ whenever $\mathbf{v} \in \mathbf{A}$, where d is the dimension of \mathcal{D} . For non-reference nodes, let $\eta^{-1}(U_i) = \mathbf{b}_i$ and $\eta^{-1}(S_i) = \mathbf{a}_i$. Then, we specify $\text{Pa}[\mathbf{b}_i] = \{\mathbf{a}_i\}$ —non-reference locations’ parent set comprises reference locations in the same domain partition. These specifications for \mathcal{G} imposes a coloring on \mathcal{G} enabling parallel sampling of the latent random effects (see, e.g., [Gonzalez et al., 2011](#)), independently of observed locations \mathcal{T} and d . At \mathcal{L} , the new process has density p^* ,

$$p^*(\mathbf{w}_{\mathcal{L}}) = \prod_{i=1}^M p(\mathbf{w}_i | \mathbf{w}_{[i]}) \prod_{\ell \in U_i} p(\mathbf{w}(\ell) | \mathbf{w}_i), \quad (8)$$

where $\mathbf{w}_i = \mathbf{w}(\eta^{-1}(\mathbf{v}_i)) = \mathbf{w}(S_i) = (\mathbf{w}(\ell_1)^\top, \dots, \mathbf{w}(\ell_{n_{S_i}})^\top)^\top$, $\mathbf{w}_{[i]} = \mathbf{w}(\eta^{-1}(\text{Pa}[\mathbf{v}_i]))$, using η^{-1} to find all reference locations mapped to the same node. We assume conditional independence at non-reference locations in this article. A Gaussian base process leads to (8) as a product of multivariate Gaussian densities; $p^*(\mathbf{w}_{\mathcal{L}})$ is then Gaussian with a sparse precision matrix – refer to [Peruzzi et al. \(2020\)](#) for more details.

For an observed location $\ell \in \mathcal{T} \cap D_i$, the standard MGP regression model is

$$\begin{aligned} \mathbf{y}(\ell) &= \mathbf{X}(\ell)^\top \boldsymbol{\beta} + \mathbf{w}(\ell) + \boldsymbol{\varepsilon}(\ell); \quad \boldsymbol{\varepsilon}(\ell) \sim N(\mathbf{0}, \mathbf{D}); \\ \mathbf{w}(\ell) &= \mathbf{H}_\ell \mathbf{w}_{[\ell]} + \boldsymbol{\xi}(\ell); \quad \boldsymbol{\xi}(\ell) \sim N(\mathbf{0}, \mathbf{R}_\ell), \end{aligned} \quad (9)$$

where, denoting $\mathbf{C}_\ell = \mathbf{C}(\ell, \ell)$, the set of parent locations as $B = \eta^{-1}(\text{Pa}[\eta(\ell)])$ and $\mathbf{C}_{[\ell]} = \mathbf{C}(B, B)$, we have $\mathbf{H}_\ell = \mathbf{C}_{\ell, [\ell]} \mathbf{C}_{[\ell]}^{-1}$ and $\mathbf{R}_\ell = \mathbf{C}_\ell - \mathbf{C}_{\ell, [\ell]} \mathbf{C}_{[\ell]}^{-1} \mathbf{C}_{[\ell], \ell}$. Since evaluating $p(\mathbf{w} | \boldsymbol{\theta})$ is required in posterior sampling of $\boldsymbol{\theta}$, the primary computing cost depends on $\mathbf{C}_{[\ell]}^{-1}$. The number of such inverses and their sizes depend on \mathcal{T} , \mathcal{S} , and \mathcal{U} , for a given \mathcal{G} and \mathcal{T} . If \mathcal{T} are gridded, we let $\mathcal{S} \supset \mathcal{T}$ be the observed grid plus the missing grid locations, and $\mathcal{U} = \emptyset$. Only $O(d)$ larger matrix inverses are needed, rather than M , and \mathbf{w} is sampled at $|\mathcal{S}|$ locations.

In fact, with stationary cross-covariances, for a given node \mathbf{v}_i one can find “prototypes” $\mathbf{v}_{i\#}$ and \mathbf{v}_{i*} such that $\mathbf{C}_i = \mathbf{C}_{i\#}$ and $\mathbf{C}_{[i]} = \mathbf{C}_{[i*]}$, and the number of prototype nodes is $O(d)$. One computes the inverses for the prototypes and copies the result across the

whole domain. If \mathcal{T} are not gridded, then we still let \mathcal{S} be a grid, again leading to $O(d)$ large matrix solvers. However, now $\mathcal{T} = \mathcal{U}$ and we sample \mathbf{w} at $|\mathcal{S}| + |\mathcal{U}|$ locations. Since $n_{\mathcal{S}} = |\mathcal{S}| \approx n$ to avoid over-smoothing the spatial surface, we would be using about twice as many latent variables as we have observations. Updates of the centered parameters proceed by evaluating $p(\mathbf{w}_{\mathcal{S}} | \boldsymbol{\theta}) \times p(\mathbf{w}_{\mathcal{U}} | \mathbf{w}_{\mathcal{S}}, \boldsymbol{\theta})$, which implies that the move from $\boldsymbol{\theta}$ to $\boldsymbol{\theta}'$ must agree with the current high-dimensional sample of the latent process at both reference and non-reference locations. Consequently, MCMC convergence will be slow. Clearly, the computational speedup of gridded reference sets may not compensate for such inefficiencies.

3 Grid, Parametrize, Split

We now generalize the computational advantages of QMGPs to non-gridded data, and rebuild the linear model of coregionalization to improve the overall sampling efficiency. We assume, without loss of generality, that the observed locations \mathcal{T} are irregularly spaced. We target raw speed in the first subsection, efficiency in the next.

3.1 Reference set on a Grid

We build the reference set \mathcal{S} as a grid, regardless of \mathcal{T} . If $\mathcal{D} = [0, 1]^d$, we may take $\mathcal{S} = \left\{ \left(\frac{j_1}{N_1}, \dots, \frac{j_d}{N_d} \right) : (j_1, \dots, j_d) \in \{1, \dots, N_d\}^d \right\}$, so the number of reference locations is $n_{\mathcal{S}} = \prod_{j=1}^d N_j$. From (9) we can partly marginalize the latent process at the observed locations. For a location $\boldsymbol{\ell} \in D_i$ and conditioning on realizations of the latent process at \mathcal{S} , we have

$$\mathbf{y}(\boldsymbol{\ell}) = \mathbf{X}(\boldsymbol{\ell})^\top \boldsymbol{\beta} + \mathbf{H}_{\boldsymbol{\ell}} \mathbf{w}_{[\boldsymbol{\ell}]} + \boldsymbol{\varepsilon}'(\boldsymbol{\ell}); \quad \boldsymbol{\varepsilon}'(\boldsymbol{\ell}) \sim N(\mathbf{0}, \mathbf{D} + \mathbf{R}_{\boldsymbol{\ell}}), \quad (10)$$

where $\mathbf{w}_{[\boldsymbol{\ell}]}$ are process realizations at locations $\eta^{-1}(\text{Pa}[\mathbf{b}_i])$ since $\boldsymbol{\ell} \in D_i$ and, hence, $\eta(\boldsymbol{\ell}) = \mathbf{b}_i$, $\mathbf{H}_{\boldsymbol{\ell}}$ and $\mathbf{R}_{\boldsymbol{\ell}}$ are $q \times n_{\mathcal{S}_i}$ and $q \times q$ matrices, respectively. For a given $\mathbf{w}_{\mathcal{S}}$, if $\boldsymbol{\ell} \in \mathcal{S}$ then $\mathbf{R}_{\boldsymbol{\ell}} = \mathbf{0}$ and $\mathbf{H}_{\boldsymbol{\ell}} \mathbf{w}_{[\boldsymbol{\ell}]} = \mathbf{w}_{\boldsymbol{\ell}}$. In other words, (10) generalizes QMGPs to nongridded data without sampling at too many locations. Furthermore, while no issue arise if \mathcal{T} and \mathcal{S} partly overlap, in general they are exclusive.

Partial marginalization of the latent process removes the need to sample at non-reference locations. However, unlike full marginalization, the advantages induced by having \mathcal{S} on a grid are maintained. Moreover, choosing a grid \mathcal{S} such that $n_{\mathcal{S}} \ll n$ leads to interpreting

(10) as a “meshed” extension of the bias-adjusted predictive process (MPP; Finley et al., 2009). While computational considerations make it advantageous to choose \mathcal{S} on a grid, (10) does not preclude alternatives. For example, typical $\mathcal{T} = \mathcal{S}$ implies prediction locations do are not in the reference set, but here—assuming $\mathbf{X}(\boldsymbol{\ell})$ are available—we can choose \mathcal{S} as the prediction set. Then, sampling $\mathbf{w}_{\mathcal{S}}$ yields the desired predictions. This feature can be used to produce model-based heat maps (i.e. raster images) of the latent process at any resolution. Finally, while partial marginalization is available for Gaussian first stage models, we expect analogous strategies to be similarly advantageous otherwise, taking advantage of conditional independence of all outcomes on the latent process.

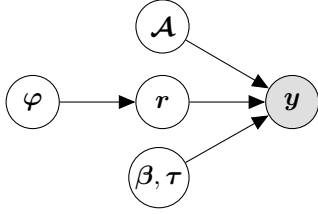
3.2 Parametrize a Matérn LMC, *Split* its variance

This subsection does not assume \mathbf{w} is a QMGP. After letting $\tilde{\boldsymbol{\omega}}(\boldsymbol{\ell}) = (\tilde{\omega}_1(\boldsymbol{\ell}), \dots, \tilde{\omega}_k(\boldsymbol{\ell}))^\top$ and $\tilde{\omega}_j(\boldsymbol{\ell}) \sim GP(0, \tilde{\mathbf{C}}_j)$, where

$$\tilde{\mathbf{C}}_j(\boldsymbol{\ell}, \boldsymbol{\ell}') = \frac{\rho(\boldsymbol{\ell}, \boldsymbol{\ell}'; \{\phi_j, \nu_j\})}{\phi_j^{2\nu_j}}, \quad (11)$$

we write the LMC as $\mathbf{w}(\boldsymbol{\ell}) = \boldsymbol{\Lambda}\boldsymbol{\omega}(\boldsymbol{\ell}) = \boldsymbol{\Lambda}\mathbf{Q}\mathbf{Q}^{-1}\boldsymbol{\omega}(\boldsymbol{\ell}) = \tilde{\boldsymbol{\Lambda}}\tilde{\boldsymbol{\omega}}(\boldsymbol{\ell})$, where $\mathbf{Q} = \text{diag}\{\phi_1^{\nu_1}, \dots, \phi_k^{\nu_k}\}$. $\tilde{\boldsymbol{\Lambda}} = \boldsymbol{\Lambda}\mathbf{Q}$ is thus a lower-triangular rescaling matrix whose j th diagonal element is $\lambda_{jj}\phi_j^{\nu_j}$, which is the square root of the microergodic parameter (Stein, 1999)—its better identifiability impacts MCMC efficiency positively. The immediate consequence of this change is that posterior samples of $\boldsymbol{\Lambda}$ will only be obtained via post-processing of MCMC output—we will instead directly sample $\tilde{\boldsymbol{\Lambda}}$ and $\tilde{\boldsymbol{\omega}}$.

The LMC is typically estimated as a noncentered parametrization, which as we mentioned is associated with poor mixing when the nuggets are small. We address this issue by parameter expansion (or splitting) of λ_{jj}^2 : denoting $\boldsymbol{\Psi} = \{\lambda_{11}, \dots, \lambda_{kk}\}$, we find $\mathbf{L} = \boldsymbol{\Lambda}\boldsymbol{\Psi}^{-1}$ as a lower triangular matrix with units along the diagonal. Letting $\mathbf{J} = \text{diag}\{\sigma_1^{-1}, \dots, \sigma_k^{-1}\}$, we write the LMC as $\mathbf{w}(\boldsymbol{\ell}) = \boldsymbol{\Lambda}\boldsymbol{\omega}(\boldsymbol{\ell}) = \mathbf{L}\boldsymbol{\Psi}\boldsymbol{\omega}(\boldsymbol{\ell})$. The split follows by writing $\mathbf{w}(\boldsymbol{\ell}) = \boldsymbol{\Lambda}\mathbf{J}\mathbf{J}^{-1}\boldsymbol{\omega}(\boldsymbol{\ell}) = \bar{\boldsymbol{\Lambda}}\bar{\boldsymbol{\omega}}(\boldsymbol{\ell})$, where $\bar{\boldsymbol{\Lambda}} = \mathbf{L}\boldsymbol{\Psi}\mathbf{J}$, $\bar{\omega}_j(\boldsymbol{\ell}) \sim GP(0, \sigma_j^2\rho_j)$ and ρ_j is as above. In practice, we sample $\bar{\boldsymbol{\omega}}$ alongside $\bar{\boldsymbol{\Lambda}}$, whose j th diagonal element is $\bar{\lambda}_{jj} = \lambda_{jj}/\sigma_j$. The split entails an overparametrization of the variances as we assign a prior on $\bar{\boldsymbol{\Lambda}}$ which is independent of the prior on \mathbf{J} . If $q = 1$, we may assign a truncated Gaussian prior on $\bar{\lambda}$ centered at zero



$$\mathbf{A} = \mathbf{\Lambda} \mathbf{Q} \mathbf{J} = \mathbf{\Lambda} \begin{bmatrix} \phi_1^{\nu_1} & & & \\ & \ddots & & \\ & & \phi_k^{\nu_k} & \\ & & & \ddots \end{bmatrix} \begin{bmatrix} \sigma_1^{-1} & & & \\ & \ddots & & \\ & & \ddots & \\ & & & \sigma_k^{-1} \end{bmatrix}$$

$$\boldsymbol{\varphi} = \{\sigma_j^2, \phi_j, \nu_j\}_{j=1}^k$$

Figure 2: DAG of the Bayesian spatial regression model using a *PS* parametrization. The relationship with a standard parametrization is summarised on the right.

with truncation below zero, and an inverse Gamma on σ^2 , to get a half-t for $\lambda = \bar{\lambda}\sigma$ (Gelman, 2006). In the context of Bayesian factor models, a similar parameter expansion was introduced in Ghosh and Dunson (2009).

4 Bayesian GriPS regression

We build the model for \mathbf{w} by combining parametrization and splitting strategies:

$$\mathbf{w}(\boldsymbol{\ell}) = \mathbf{\Lambda} \boldsymbol{\omega}(\boldsymbol{\ell}) = \mathbf{\Lambda} \mathbf{Q} \mathbf{J} \mathbf{J}^{-1} \mathbf{Q}^{-1} \boldsymbol{\omega}(\boldsymbol{\ell}) = \mathbf{A} \mathbf{r}(\boldsymbol{\ell}), \quad (12)$$

where $\mathbf{A} = \mathbf{\Lambda} \mathbf{Q} \mathbf{J}$ is a $q \times k$ matrix with zeros in the upper triangular part, the k -variate process is $\mathbf{r}(\cdot) \sim \text{QMGP}(\mathbf{0}, \mathbf{K}(\cdot))$ such that $\mathbf{r}(\boldsymbol{\ell}) = (r_1(\boldsymbol{\ell}), \dots, r_k(\boldsymbol{\ell}))^\top$ and, for each $j = 1, \dots, k$, $r_j(\boldsymbol{\ell}) \sim \text{QMGP}(0, K_j(\cdot))$ where $K_j(\cdot) = \sigma_j^2 \frac{\rho_j(\cdot)}{\phi_j^{2\nu_j}}$ with $\rho_j(\cdot)$ as the Matérn correlation in (5). All independent QMGPs are built on the same domain partition \mathbf{T} and the same graph \mathcal{G} . The GriPS spatial regression model then becomes

$$\mathbf{y}(\boldsymbol{\ell}) = \mathbf{X}(\boldsymbol{\ell})^\top \boldsymbol{\beta} + \mathbf{Z}_\ell \mathbf{r}_{[\ell]} + \boldsymbol{\varepsilon}'(\boldsymbol{\ell}); \quad \boldsymbol{\varepsilon}'(\boldsymbol{\ell}) \sim N(\mathbf{0}, \mathbf{D} + \boldsymbol{\Sigma}_\ell), \quad (13)$$

where $\mathbf{Z}_\ell = \mathbf{A} \mathbf{H}_\ell$, $\boldsymbol{\Sigma}_\ell = \mathbf{A} \mathbf{R}_\ell \mathbf{A}^\top$. Writing (13) for locations \mathcal{T} , we get

$$\mathbf{y} = \mathbf{X} \boldsymbol{\beta} + \mathbf{Z} \mathbf{r} + \boldsymbol{\varepsilon}'; \quad \boldsymbol{\varepsilon}' \sim N(\mathbf{0}, \mathbf{D}_n + \boldsymbol{\Sigma}), \quad (14)$$

where \otimes denotes the Kronecker product, $\mathbf{Z} = (\mathbf{I}_n \otimes \mathbf{A}) \mathcal{H}$, and $\boldsymbol{\Sigma} = (\mathbf{I}_n \otimes \mathbf{A}) \mathcal{R} (\mathbf{I}_n \otimes \mathbf{A}^\top)$. In addition to the terms already appearing in (2), we now explicitly have \mathbf{r} representing the $nk \times 1$ vector of latent effects at the gridded reference set \mathcal{S} . Furthermore, \mathcal{H} is a sparse $nk \times n_{\mathcal{S}}k$ matrix whose i th row block is filled with \mathbf{H}_{ℓ_i} , with zeroes at columns corresponding to locations in \mathcal{S} not in the parent set of ℓ_i . Since the k margins of the \mathbf{r}

process are independent, the permutation of the columns of \mathbf{H}_{ℓ_i} that arranges it according to the process margins is a block-diagonal matrix whose j th (of the total k) row block is $K_j(\boldsymbol{\ell}, [\boldsymbol{\ell}])K_j^{-1}([\boldsymbol{\ell}])$. Similarly, \mathbf{R} is a diagonal $nk \times nk$ matrix whose i th block is \mathbf{R}_{ℓ_i} , itself diagonal with j th diagonal element $K_j(\boldsymbol{\ell}, \boldsymbol{\ell}) - K_j(\boldsymbol{\ell}, [\boldsymbol{\ell}])K_j^{-1}([\boldsymbol{\ell}])K_j([\boldsymbol{\ell}], \boldsymbol{\ell})$. We find $\boldsymbol{\Sigma}$ as a block-diagonal matrix of dimension $nq \times nq$ with $q \times q$ blocks—the i th block is $\mathbf{A}\mathbf{R}_{\ell_i}\mathbf{A}^\top$.

We complete the Bayesian model by assigning multivariate Gaussian prior distributions to $\boldsymbol{\beta}$ and the lower triangular elements of \mathbf{A} , and independent zero-mean Gaussian distributions truncated below zero for the diagonal elements of \mathbf{A} . We also assign independent Inverse Gamma priors for each σ_j^2 , $j = 1, \dots, k$ and each τ_i^2 , $i = 1, \dots, q$. Figure 2 summarises the *PS* parametrization—GriPS regressions are noncentered on \mathbf{A} and centered on $\boldsymbol{\varphi} = \{\sigma_j^2, \phi_j, \nu_j\}_{j=1}^k$. Ultimately, we are interested in $\boldsymbol{\Lambda} = \mathbf{A}\mathbf{J}^{-1}\mathbf{Q}^{-1}$, meaning that a *PS* parametrization is simultaneously centered and noncentered on $\boldsymbol{\Lambda}$ since \mathbf{J} and \mathbf{Q} include the centered parameters. Next, we outline the sampling algorithms for estimation and prediction.

4.1 Estimation and prediction

Updating \mathbf{r} proceeds following \mathcal{G} . Taking reference node $\mathbf{v}_i \in \mathbf{A}$, the set T_i are locations having S_i as parent set, hence we can write $\mathbf{y}_{T_i} = \mathbf{X}_{T_i}\boldsymbol{\beta} + \mathbf{Z}_{T_i}\mathbf{r}_i + \boldsymbol{\varepsilon}_{T_i}$ and $\boldsymbol{\varepsilon}_{T_i} \sim N(\mathbf{0}, \mathbf{D}_{T_i} + \boldsymbol{\Sigma}_{T_i})$. Denote $\tilde{\mathbf{y}}_{T_i} = \mathbf{I}_{T_i}(\mathbf{y}_{T_i} - \mathbf{X}_{T_i}\boldsymbol{\beta})$ and $\tilde{\mathbf{D}}_{T_i} = \mathbf{I}_{T_i}(\mathbf{D}_{T_i} + \boldsymbol{\Sigma}_{T_i})\mathbf{I}_{T_i}$, where \mathbf{I}_{T_i} is a diagonal matrix with zeros at elements corresponding to missing outcomes in T_i , ones elsewhere. Calling $\text{Ch}[\mathbf{v}_i] = \{\mathbf{v}_j : \mathbf{v}_i \in \text{Pa}[\mathbf{v}_j]\}$, we partition $\mathbf{H}_j = [\mathbf{H}_i : \mathbf{H}_{[j]\setminus i}]$ for each $\mathbf{v}_j \in \text{Ch}[\mathbf{v}_i]$, and similarly $\mathbf{r}_{[j]} = (\mathbf{r}_i^\top, \mathbf{r}_{[j]\setminus i}^\top)^\top$, where the $[j] \setminus i$ notation refers the set $\text{Pa}[\mathbf{v}_j] \setminus \{\mathbf{v}_i\}$. Then, the full conditional distribution of \mathbf{r}_i is Gaussian, with mean \mathbf{g}_i and covariance \mathbf{G}_i such that:

$$\begin{aligned} \mathbf{G}_i^{-1} &= \mathbf{Z}_{T_i}^\top \tilde{\mathbf{D}}_{T_i}^{-1} \mathbf{Z}_{T_i} + \mathbf{R}_i^{-1} + \sum_{j \in \text{Ch}[\mathbf{v}_i]} \mathbf{H}_{[j]\setminus i}^\top \mathbf{R}_j^{-1} \mathbf{H}_{[j]\setminus i} \\ \mathbf{G}_i \mathbf{g}_i &= \mathbf{R}_i^{-1} \mathbf{H}_i \mathbf{r}_{[i]} + \mathbf{Z}_{T_i}^\top \tilde{\mathbf{D}}_{T_i}^{-1} \tilde{\mathbf{y}}_{T_i} + \sum_{j \in \text{Ch}[\mathbf{v}_i]} \mathbf{H}_{[j]\setminus i}^\top \mathbf{R}_j^{-1} \mathbf{r}_{[j]\setminus i}. \end{aligned}$$

Updating $\boldsymbol{\beta}$ proceeds via its full conditional distribution, which is $N(\boldsymbol{\beta}; \mathbf{m}_\beta^{(n)}, \mathbf{V}_\beta^{(n)})$, where $\mathbf{V}_\beta^{(n)-1} = \mathbf{V}_\beta^{-1} + \mathbf{X}^\top (\mathbf{D}_n + \boldsymbol{\Sigma})^{-1} \mathbf{X}$ and $\mathbf{V}_\beta^{(n)} \mathbf{m}_\beta^{(n)} = \mathbf{V}_\beta^{-1} \mathbf{m}_\beta + \mathbf{X}^\top (\mathbf{D}_n + \boldsymbol{\Sigma})^{-1} (\mathbf{y} - \mathbf{Z}\mathbf{r})$. Updates for other unknowns may proceed via Metropolis steps: for \mathbf{A} and $\boldsymbol{\tau}$, the centered parametrization results in being target density being the prior $\pi(\mathbf{A})\pi(\boldsymbol{\tau})$, multiplied by the

following product of multivariate Gaussians

$$\prod_{i \in \mathcal{T}} N(\mathbf{y}_{\ell_i}; \mathbf{X}_{\ell_i} \boldsymbol{\beta} + \mathbf{Z}_{\ell_i} \mathbf{r}_{\ell_i}, \mathbf{D} + \boldsymbol{\Sigma}_{\ell_i}) \Big|_{\text{obs}}, \quad (15)$$

where we restrict each term to the observed outcomes, i.e. each term is an l -dimensional Gaussian corresponding to the $l \leq q$ observed outcomes at spatial location ℓ_i .

For $\boldsymbol{\varphi} = \{\sigma_j^2, \phi_j, \nu_j\}_{j=1}^k$, the Metropolis update following the centered parametrization targets the density obtained by multiplying the prior $\pi(\boldsymbol{\varphi})$ to $\prod_i^M N(\mathbf{r}_i; \mathbf{H}_i \mathbf{r}_{[i]}, \mathbf{R}_i)$, which translates (8) for the GriPS coregionalization model. In our implementation, we use the robust adaptive Metropolis algorithm of Vihola (2012) to target an acceptance rate of about 0.23. We note that it is computationally easier to update \mathcal{A} , $\boldsymbol{\tau}$ and $\boldsymbol{\sigma}^2$ than $\boldsymbol{\phi}$ and $\boldsymbol{\nu}$ as the latter two require recomputing the correlations. Finally, if \mathcal{T} is an incomplete grid and we choose $\mathcal{S} \supset \mathcal{T}$ as the grid which “fills the gaps” in \mathcal{T} , then the regression error is $\boldsymbol{\varepsilon} \sim N(\mathbf{0}, \mathbf{D}_n)$. In that case, with the prior distributions we have mentioned earlier, \mathcal{A} and $\boldsymbol{\tau}$ can be updated via their full conditionals—refer to the supplementary material for details. If $\mathcal{S} \neq \mathcal{T}$, then those full conditionals are the correct updates for posterior sampling of model $\mathbf{y} = \mathbf{X}\boldsymbol{\beta} + \mathbf{Z}\mathbf{r} + \tilde{\boldsymbol{\varepsilon}}$ where $\tilde{\boldsymbol{\varepsilon}} \sim N(0, \mathbf{D}_n)$, which is not (14) as $\boldsymbol{\Sigma}$ is omitted and is instead akin to a meshed version of the “unmodified” predictive process of Banerjee et al. (2008); we expect the performance of the two models to be very similar when \mathcal{S} is large and $\mathcal{S} \supset \tilde{\mathcal{S}} \approx \mathcal{T}$. All applications in this article use Metropolis updates for (14) on nongridded data.

4.2 Applications on synthetic data

We illustrate the performance of GriPS in estimation and prediction in univariate spatial regressions using simulated data. Each generated data set includes a realization of a Gaussian process with Matérn covariance (5), fixing the smoothness ν to its known value (either $\nu = 0.5$ or $\nu = 1.5$). The outcomes are observed at irregularly-spaced locations in $[0, 1]^2$. The total number of observed locations is $n = 5000$. Our main goal is the efficient estimation of the posterior distribution of σ^2, ϕ, τ^2 . Predictive performance is used to validate our methodology. We use a grid of $n_{\text{out}} = 10000$ spatial locations as our test set. We set \mathcal{S} in GriPS models to overlap with the test set—we are thus sampling the spatial process at twice as many locations as there are observations. For $\nu = 0.5$, we generate 50 datasets for each

<i>Efficiency</i>		$\nu = 0.5$			$\nu = 1.5$		
		ESS	ESS/s	Relative	ESS	ESS/s	Relative
QMGP GriPS	ϕ	245.46	12.78	52.11	125.40	6.49	50.59
	σ^2	248.68	12.95	49.04	224.83	11.68	97.44
	τ^2	116.04	6.04	1.38	231.46	12.03	6.68
QMGP latent	ϕ	4.46	0.19	0.78	4.84	0.28	2.16
	σ^2	5.88	0.25	0.95	7.34	0.42	3.51
	τ^2	206.54	8.78	2.00	356.89	20.50	11.39
NNGP response	ϕ	11.30	0.25	1.00	23.00	0.13	1.00
	σ^2	12.17	0.26	1.00	21.45	0.12	1.00
	τ^2	201.44	4.38	1.00	310.28	1.80	1.00
NNGP latent	ϕ	5.81	0.09	0.38	3.88	0.02	0.16
	σ^2	8.39	0.13	0.51	7.56	0.04	0.33
	τ^2	207.61	3.33	0.76	71.34	0.37	0.21

Table 1: MCMC efficiency of GriPS in the estimation of Matérn parameters in univariate settings. For posterior samples of size 2500, we report effective sample size—absolute, per unit time, and relative to the NNGP response model.

combination of $\sigma^2 \in \{1, 5\}$ and $\phi \in \{0.5, 5\}$, and similarly for $\nu = 1.5$ but with $\phi \in \{5, 25\}$, for a total of 400 datasets each of size $n_{\text{all}} = 15000$.

QMGP based on GriPS are compared with unmodified “latent” QMGPs and NNGPs, both of which also sample the latent process, but without reparametrization or splitting. We also consider a “response” NNGP model which avoids sampling the latent process, and a stochastic partial differential equations approach (Lindgren et al., 2011) via integrated nested Laplace approximations (INLA; Rue et al., 2009) that avoids MCMC altogether. The SPDE-INLA approach scales to big data via a sparse GMRF approximation of the Gaussian field which requires the user to define a mesh of points. We fix the mesh at the test set—also the reference set in GriPS. Carefully assessing MCMC convergence for each of the 400 datasets is impractical. Hence, we fix the number of iterations to 5000 for all MCMC-based methods. In these settings, GriPS is almost always faster in computing 5000 MCMC iterations than the non sampling-based INLA SPDE method on the same task. We provide more details on the implemented methods in the supplementary material, along with additional figures and

<i>Estimation</i>		$\nu = 0.5$			$\nu = 1.5$		
		RMSE	M%E	UQ: Covg	RMSE	M%E	UQ: Covg
QMGP GriPS	ϕ	1.1705	0.7463	0.8100	1.9102	0.1176	0.6850
	σ^2	1.8981	0.3764	0.8350	1.8311	0.3332	0.8600
	τ^2	0.0048	0.0628	0.9450	0.0015	0.0239	0.9600
QMGP latent	ϕ	1.7042	0.8251	0.6450	1.9753	0.1581	0.8600
	σ^2	4.3575	0.9618	0.6400	4.9800	0.6827	0.8500
	τ^2	0.0069	0.0955	0.7150	0.0018	0.0282	0.9200
NNGP response	ϕ	1.4851	1.0549	0.5500	1.5224	0.1494	0.7450
	σ^2	1.9187	0.4221	0.5450	1.4961	0.2743	0.7150
	τ^2	0.0050	0.0649	0.8650	0.0015	0.0227	0.9500
NNGP latent	ϕ	1.2829	0.9697	0.5150	7.6886	1.0344	0.3700
	σ^2	2.0355	0.4059	0.5100	2.6931	0.5092	0.4400
	τ^2	0.0059	0.0754	0.7950	2.9921	27.3383	0.3350
SPDE INLA	ϕ	6.1887	6.0161	0.0000	unsupported in R-INLA		
	σ^2	2.5137	0.6386	0.0050			
	τ^2	0.0520	0.7080	0.0050			

Table 2: Accuracy in estimating the Matérn parameters ϕ, σ^2, τ^2 in univariate settings: root mean square error (*RMSE*), mean absolute percentage error (*M%E*), and uncertainty quantification in terms of coverage (*UQ: Covg*, with target 95%), averaged across 400 datasets.

<i>Prediction</i>	$\nu = 0.5$			$\nu = 1.5$		
	RMSPE	CRPS	UQ: Covg	RMSPE	CRPS	UQ: Covg
QMGP-GriPS	0.3489	0.1960	0.9445	0.2651	0.1490	0.9478
QMGP latent	0.3512	0.1967	0.9509	0.2677	0.1503	0.9438
NNGP response	0.3474	0.1955	0.9464	0.2709	0.1523	0.9350
NNGP latent	0.3462	0.1945	0.9476	0.8003	0.5244	0.9723
SPDE-INLA	0.3462	0.1948	0.9602	unsupported in R-INLA		

Table 3: Accuracy in predictions at 10000 unobserved locations, averaged across 400 datasets, measured as root mean square prediction error (*RMSPE*), continuous ranked probability score (*CRPS*), and uncertainty quantification measured as coverage of 95% prediction intervals.

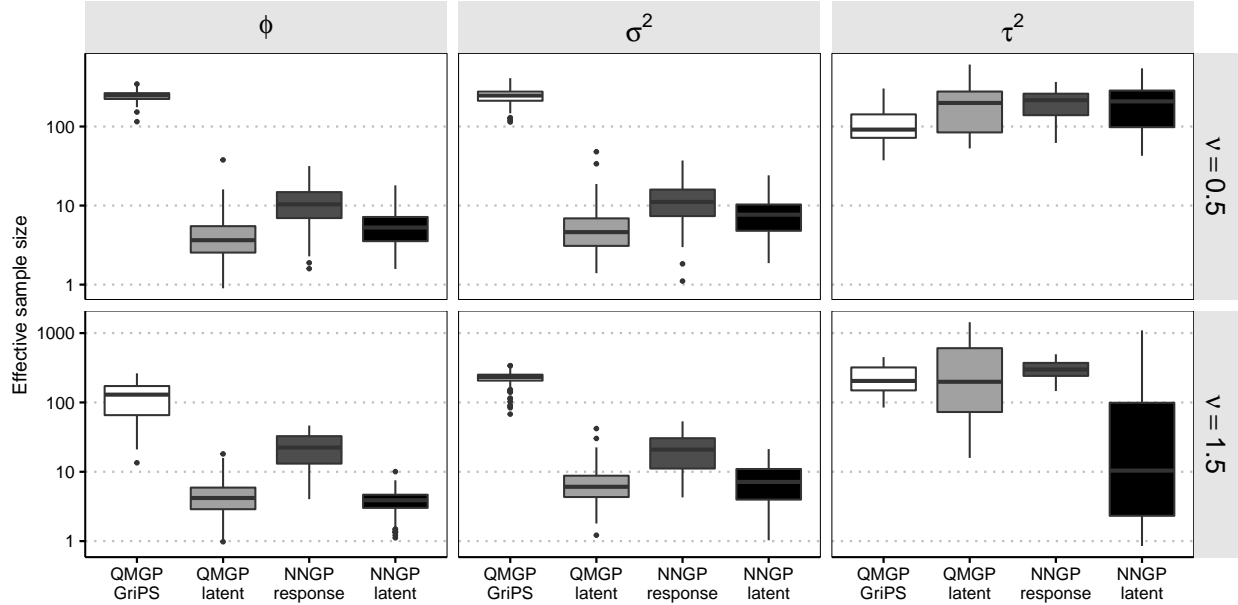


Figure 3: Effective sample size (log-scaled) in estimating σ^2 , ϕ , τ^2 at different Matérn smoothness ($\nu = 0.5$ or $\nu = 1.5$), from an MCMC sample of size 2500.

summaries of computing time for each approach.

Sampling efficiency in terms of effective sample size per unit time is shown in Table 1. As expected, the “latent” NNGP method is less efficient than its “response” counterpart. The latter displays performance similar to the unmodified QMGP model. On the other hand, the GriPS method is massively more efficient than all other methods when estimating σ^2 and ϕ —the relative efficiency improvements are between one and two orders of magnitude.

These efficiency improvements are reflected in the accuracy of estimations, as shown in Table 2. In particular, GriPS provide more reliable uncertainty quantification as evidenced by the better coverage of the posterior 95% credible intervals (uncertainty intervals for all 400 data sets are reported in the supplementary material). Furthermore, GriPS-based methods most accurately estimate the exponential covariance parameters, with the smoother $\nu = 1.5$ slightly favoring an NNGP response model. However, in the latter scenario GriPS still achieves the best predictive performance, as shown in Table 3.

We have, thus far, considered unmodified QMGPs in our comparison, which use $\mathcal{S} = \mathcal{T}$ with irregularly spaced locations. As a consequence, the net effect of the PS parametrization alone is unclear. We address this matter in the supplementary material by considering gridded data, in which case all QMGP models use the same reference set and thus all

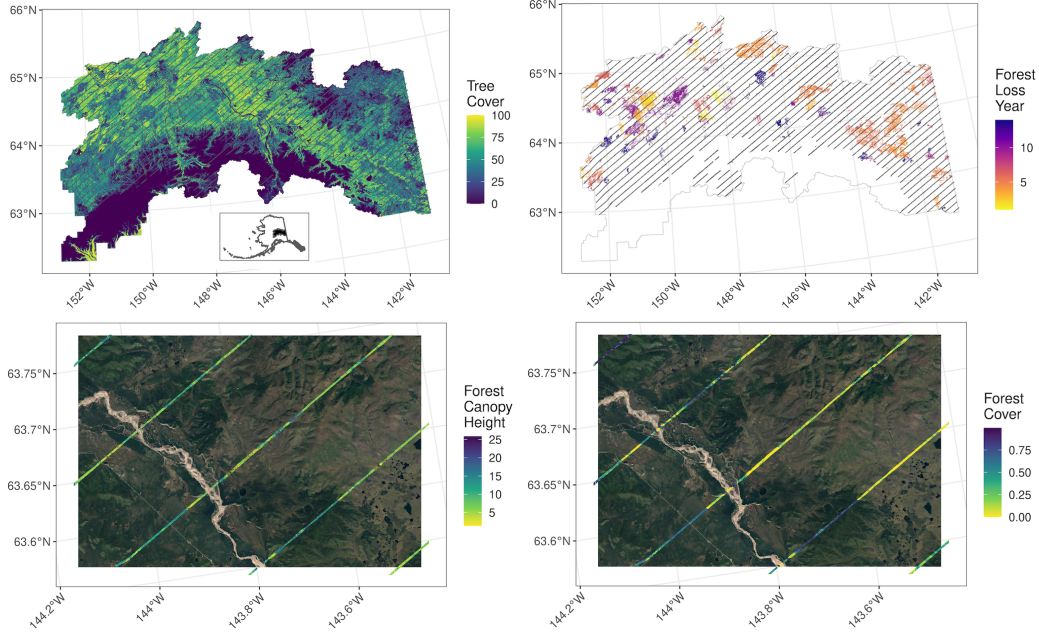


Figure 4: At the top: tree cover in 2000 (left) and forest loss year (right) over the entire study area. At the bottom: the two outcomes ($p.90$ and $f.cvr$) shown at a smaller subregion. The strips along which the outcomes are recorded appear as thin lines in the top maps.

performance differences will be attributable to the PS parametrization. The results of our analysis show that the efficiency improvements due to PS are even larger than shown in this section, and QMGP-GriPS is shown to be more than two orders of magnitude more efficient than an NNGP model of the response in estimating σ^2 and ϕ .

5 Alaskan LiDAR data

We consider a large set of remotely sensed light detection and ranging (LiDAR) data, collected using the National Aeronautics and Space Administration (NASA) Goddard’s LiDAR, Hyperspectral, and Thermal (G-LiHT) Airborne Imager (Cook et al., 2013) sensor in Summer 2014 over a large region in Alaska. The data set includes observations of forest canopy height (labeled $p.90$ and measured in meters) and fractional forest cover ($f.cvr$) at 12,270,334 spatial locations, which we seek to jointly characterize in a multivariate regression model. Owing to the low flying altitude (355m) and narrow field of view (30°) of the sensor, the observed data locations are not uniformly spread out in the study area. Instead, they are

highly concentrated along swaths less than 200m wide and separated by 9km of unobserved areas. This data set has been considered in the context of univariate spatial regressions in [Finley et al. \(2019\)](#), to which we refer for additional details.

We select a sub-region of the data of size $150\text{km} \times 250\text{km}$ covering about 31.2% of the observed data, and sample 2.5 million spatial locations uniformly at random in this area to build the data set we consider. The resulting study area includes 17 strips of observed data. The effective dimension of our data is thus $nq = 5 \times 10^6$ accounting for $q = 2$. We seek to make predictions of both outcomes on the full sub-region (including the wide areas separating the observed strips) based on the spatial regression model (14) and using two covariates that are available across the entire study area as shown in Figure 4. The two covariates are: (i) percent forest cover measured in the year 2000 (labeled tc); and (ii) an indicator variable of forest loss ($loss$) that gives the number of years since 2000 that a location had a forest-destroying disturbance such as a fire. Outcomes and predictors are shown in Figure 4.

We build the reference set \mathcal{S} for GriPS by taking a grid (colored in orange in Figure 5) of regularly-spaced locations. Its size is $n_{\text{orange}} = 1.52 \times 10^6$ which we use to cover the selected study area. However, this grid is not dense enough to accurately characterize spatial dependence since only a small portion of the reference locations are near the observed outcomes. For this reason, we augment \mathcal{S} with an additional patterned grid (colored in blue in Figure 5)—of size $n_{\text{blue}} = 5.44 \times 10^5$ —that is built to cover the 17 strips, but not the unobserved areas. Rather than aiming for perfectly overlapping this grid with the data, we create a regular pattern of blue strips by equally spacing their centers. The slight off-centering of some data swaths along this pattern motivates us to expand each grid strip symmetrically in both directions.

We implement the QMGP model on \mathcal{S} by partitioning the coordinates into 33 and 500 intervals, respectively. This patterned setup ensures that only a few matrix inverses have to be computed at each iteration. Given that $p.90 > 0$ and $0 < f.cvr < 1$, we fit (14) on $\widetilde{p.90} = \log\{p.90\}$ and analogously take $\widetilde{f.cvr} = \log\{f.cvr/(1 - f.cvr)\}$. We ran MCMC for a total of 20,000 iterations, of which we discarded the first 5,000 as burn-in. Predictions on a test set made of 10,000 left-out observations are based on a thinned chain consisting of a total of 500 samples—memory constraints inhibit storage of a significantly larger number of

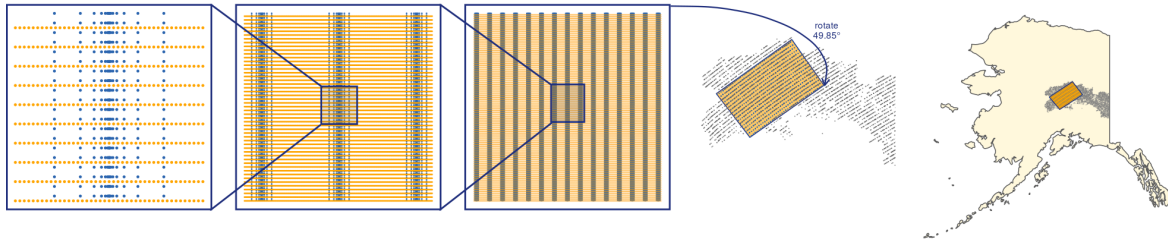


Figure 5: Construction of \mathcal{S} by overlaying a grid of regularly-spaced locations (orange) to a patterned grid (blue); alignment with the data swaths is achieved by rotating \mathcal{S} .

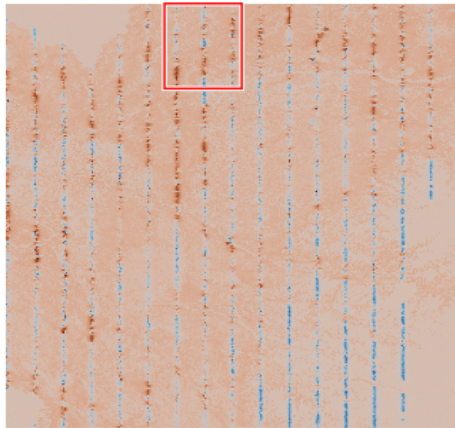
samples—and shown in Table 5. Full prediction maps over the whole study areas along with uncertainty bands are shown in Figure 6. All predictions and their summaries have been performed after inverse-transforming all posterior samples from MCMC.

We implement GriPS on two alternative partitions of the spatial domain. The first partitioning scheme tessellates the domain into 33 intervals along the horizontal and 500 along the vertical axis, resulting in a coarse partitioning of \mathcal{S} . The second uses the same partitioning for the horizontal axis, but 1000 intervals for the vertical axis. Prediction results from the two implementations are reported in Table 5. All other figures and tables refer to the coarse partition (33×500) model. We observe that the coarser partitioning strategy is conservative as it results in relatively large regions including up to 140 spatial locations. Finer partitioning leads to faster computations at a minor cost in terms of predictive accuracy. Finally, Table 4 provides marginal summaries of the posterior distribution of the unknown covariance and regression parameters. Marginal posterior densities and the full Markov chains are available in the Appendix. We find that *loss* has a negative impact on both outcomes even after accounting for spatial variability via the bivariate latent process. The two margins are positively associated as evidenced by the positive value of the off-diagonal term of $\mathbf{\Lambda}$ (their correlation at a distance $\mathbf{h} = 0$ is estimated to be about ~ 0.686).

6 Discussion

We have introduced a Grid-Parametrize-Split (GriPS) strategy for resolving inefficiencies in MCMC sampling of spatial regression models and demonstrated its validity as an alternative

Forest Canopy Height ($p.90$)



Forest Cover ($f.cvr$)

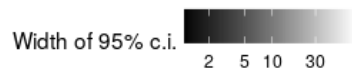
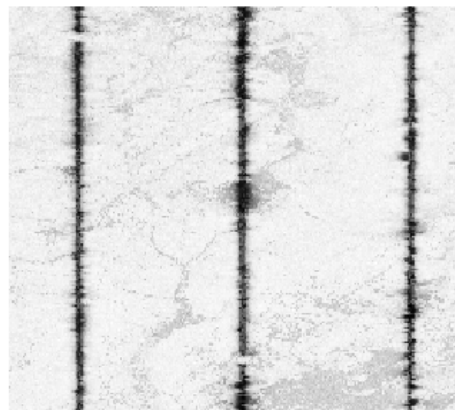
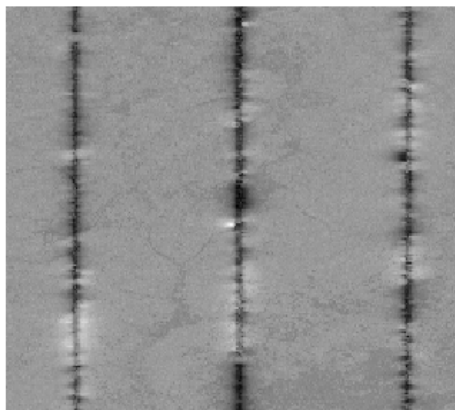
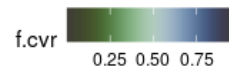
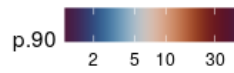
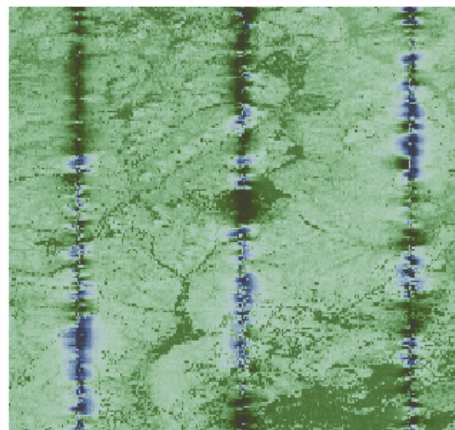
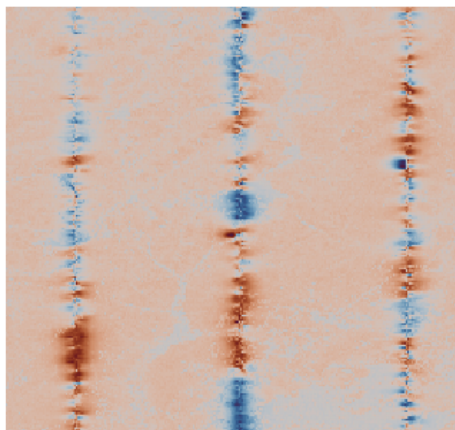
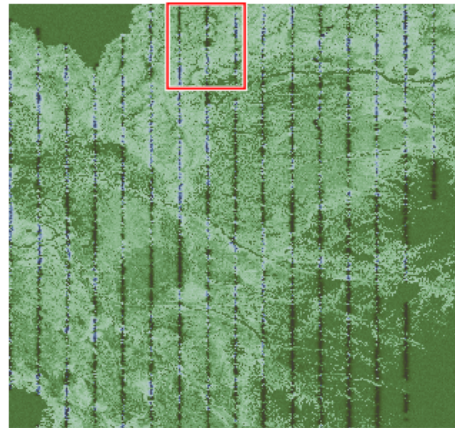


Figure 6: Predictions of $p.90$ and $f.cvr$ and uncertainty quantification in terms of the width of 95% credible intervals.

θ	$\lambda_{p.90}$	$\phi_{p.90}$	$\lambda_{f.cvr}$	$\phi_{f.cvr}$	$\lambda_{p.90,f.cvr}$
2.5% quantile	0.5085	232.5055	1.1588	357.3680	1.0777
mean	0.5213	246.4702	1.1798	376.1024	1.1118
97.5% quantile	0.5354	259.7343	1.2012	395.0176	1.1488

β and τ^2	β_{tc}	β_{tc}	β_{loss}	β_{loss}	$\tau_{p.90}^2$	$\tau_{f.cvr}^2$
	(on <i>p.90</i>)	(on <i>f.cvr</i>)	(on <i>p.90</i>)	(on <i>f.cvr</i>)		
2.5% quantile	0.0032	0.0162	-0.0018	-0.0192	0.0157	0.1325
mean	0.0032	0.0163	-0.0017	-0.0187	0.0163	0.1430
97.5% quantile	0.0033	0.0164	-0.0015	-0.0182	0.0171	0.1533

Table 4: Estimated posterior summaries for unknown covariance parameters θ , regression coefficients β , and measurement errors τ^2 for the GriPS regression on the Alaskan LiDAR data set.

	300 \times 500 partition		33 \times 1000 partition	
	<i>p.90</i>	<i>f.cvr</i>	<i>p.90</i>	<i>f.cvr</i>
RMSPE	1.7045	0.1181	1.7320	0.1197
Covg (95%)	0.9396	0.9384	0.9400	0.9401
Time/iteration	8.18s		3.98s	
Num. iterations	20,000		30,000	
Total time	45.46h		33.17h	

Table 5: Prediction results over the test set, and timing, of the two implemented models.

to methods not based on sampling the latent process a posteriori. Our development of the methodology and the subsequent numerical experiments cogently illustrate the effectiveness of GriPS in conducting spatial big data analysis. Our focus on MGPs, Matérn covariances and LMCs, and Gaussian outcomes suggests several possible directions for future research. On one hand, we expect our insight to be applicable more generally to Bayesian estimation of spatial regressions with latent processes (not necessarily MGPs). Moreover, research may focus on efficient Bayesian parametrizations of covariance models alternative to the Matérn and/or the LMC (see, e.g., [Gneiting et al., 2010](#); [Genton and Kleiber, 2015](#); [Zhang and Banerjee, 2020](#)), and on applying similar ideas to non Gaussian outcomes.

Other natural extensions include adapting DAG-based processes to spatial-temporal data analysis. Challenges specific to spatial-temporal domains include the identifying “neighbors” over space and time as the scale of associations along space significantly differ from that along time. Dynamic NNGPs ([Datta et al., 2016b](#)) resolve this problem by estimating neighbors instead of fixing them. QMGPs have been implemented on spatiotemporal domains ([Peruzzi et al., 2020](#)), but efficient estimation of the covariance parameters via MCMC remains challenging. Therefore, extensions of GriPS to spatial-temporal domains could circumvent some of these problems and can, possibly, provide easier and more effective analysis of spatial-temporal big data.

Funding

M.P. and D.B.D. have received funding from the European Research Council (ERC) under the European Union’s Horizon 2020 research and innovation programme (grant agreement No 856506), and grant R01ES028804 of the United States National Institutes of Health (NIH). A.O.F. received funding from the U.S. National Science Foundation (NSF) grants DMS-1916395 and EF-1253225, and NASA Carbon Monitoring System program. S.B. received funding from the National Science Foundation (NSF) through grants NSF/DMS 1916349 and NSF/IIS 1562303, and from the National Institute of Environmental Health Sciences (NIEHS) through grants R01ES030210 and R01ES027027.

A Full conditional updates of \mathcal{A} and τ^2

If the data are gridded or we sample \mathbf{r} at non-reference locations, full conditionals for \mathcal{A} and τ are available. Let \mathbf{Y} be the $n \times q$ matrix whose j th column is $\mathbf{Y}_j = \mathbf{y}_j - \mathbf{X}_j\boldsymbol{\beta}_j$, i.e. the j th outcome at locations \mathcal{T} , minus the static linear predictor for the same outcome. Similarly denote as \mathbf{F} the $n \times k$ matrix whose j th column is the j th margin of the \mathbf{r} process. We can then write $\mathbf{Y} = \mathbf{F}\mathcal{A}^\top + \mathbf{E}$ where \mathbf{E} is a $n \times q$ matrix such that $\text{vec}\{\mathbf{E}\} \sim N(\mathbf{0}, I_n \otimes \mathbf{D})$, with $\text{vec}\{\cdot\}$ the vectorization operator. For outcome j , let $\mathbf{F}_{(j)}$ subset \mathbf{F} to columns corresponding to the nonzero elements in the j th row of \mathcal{A} , denoted as $\mathcal{A}_{j \setminus 0}$. Then, with $\mathbf{D} = \text{diag}\{\tau_1^2, \dots, \tau_q^2\}$ the full conditional distribution of τ_j^2 is *InvGamma*(a_j^*, b_j^*) whose parameters are $a_j^* = a + n_j/2$ and $b_j^* = b + \frac{1}{2}\hat{\mathbf{E}}_j^\top \hat{\mathbf{E}}_j$, where $\hat{\mathbf{E}}_j = \mathbf{Y}_{j,\text{obs}} - \mathbf{F}_{(j),\text{obs}}\mathcal{A}_{j \setminus 0}^\top$ and $\mathbf{Y}_{j,\text{obs}}$ is the $n_j \times 1$ vector collecting the observed elements of \mathbf{Y}_j . Finally, $\mathcal{A}_{j \setminus 0}$ has Gaussian full conditional distribution with precision $\mathbf{V}_{\mathcal{A}_j}^{(n)-1} = \mathbf{V}_{\mathcal{A}_j}^{-1} + \mathbf{F}_{(j),\text{obs}}^\top (I_{n_j} \otimes \mathbf{D}^{-1}) \mathbf{F}_{(j),\text{obs}}$ and mean $\mathbf{m}_{\mathcal{A}_j}^{(n)} = \mathbf{V}_{\mathcal{A}_j}^{(n)} \mathbf{F}_{(j),\text{obs}}^\top (I_{n_j} \otimes \mathbf{D}^{-1}) \mathbf{Y}_{j,\text{obs}}$.

B Comparisons on synthetic gridded data

We compare QMGP-GriPS to unmodified QMGPs and NNGP models of the response on gridded data. Since the data grid can be directly used as reference set, we can write $\mathbf{y}(\boldsymbol{\ell}) = \mathbf{X}^\top \boldsymbol{\beta} + \mathbf{w}(\boldsymbol{\ell}) + \boldsymbol{\varepsilon}(\boldsymbol{\ell})$ where $\boldsymbol{\varepsilon}(\boldsymbol{\ell}) \sim N(\mathbf{0}, \mathbf{D})$ and we will therefore not need to modify QMGPs. We thus relabel GriPS as QMGP-PS in this section.

While the overall simulation design is the same as in the main article, here we sample the univariate Gaussian process with Matérn covariance at $n = 15625$ spatial locations on a 125×125 grid using $\mathcal{D} = [0, 1]^2$ as our spatial domain. Then, all process realizations inside the $[0.45, 0.55]^2$ region and at about 10% of the remaining locations (chosen uniformly at random) are removed from the data and considered as test set for predictions. All other design choices remain the same, implying that once again our comparisons are based on 400 datasets.

We report MCMC efficiency summaries in Table 6 and estimation and prediction results in Table 7. Compared to the synthetic data analysis in the main article and relative to unmodified QMGPs, there is only a slight improvement in QMGP-PS relative to QMGP-GriPS.

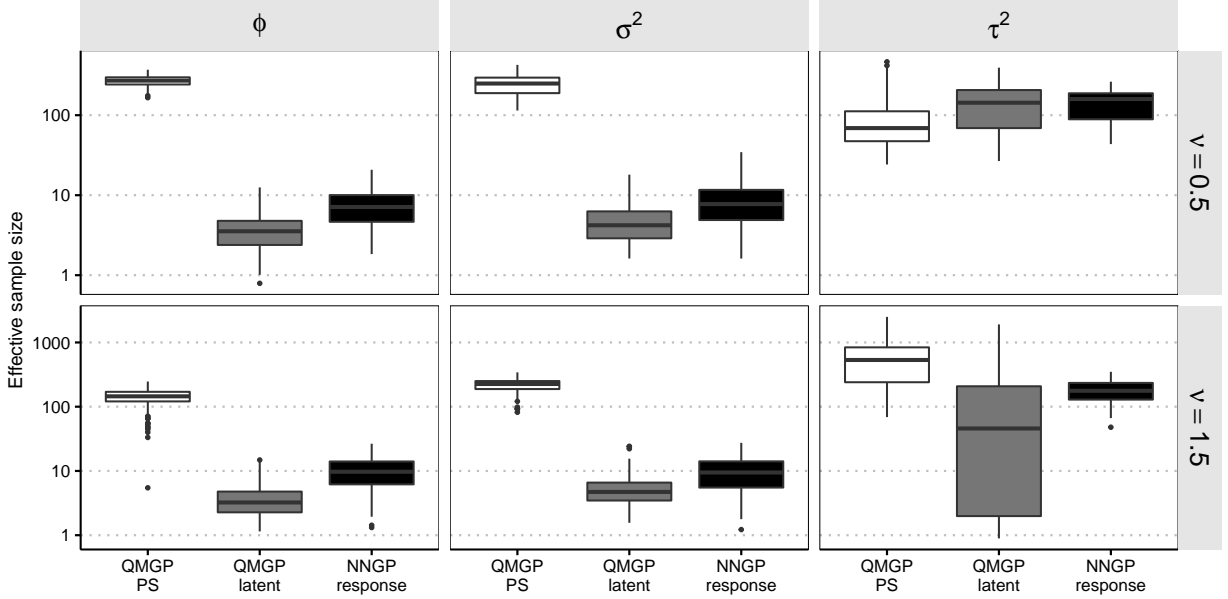


Figure 7: Effective sample size in the gridded synthetic data application.

This is a positive result for GriPS since it implies the loss in performance when choosing $\mathcal{S} \neq \mathcal{T}$ is only minor, and attributes most of the improvements to the *PS* parametrization. Furthermore, the simplifications arising in QMGPs from gridded data result in much faster computations. Relative to NNGP models of the response, we show here an *additional* 2-fold (or larger) improvement in MCMC efficiency, compared to the nongridded data setting. Estimation and prediction accuracy shown in Table 7 largely overlap with the nongridded data setting.

C Details on implemented models

In the synthetic data applications, the prior distributions on τ^2 was chosen as an inverse Gamma with parameters 2.01 and 1 for QMGP-GriPS latent QMGPs, and both NNGP models. $\pi(\sigma^2) = \text{Inv.Gamma}(2.01, 1)$ for latent QMGPs and NNGPs, whereas in GriPS this parameter is expanded into σ^2 with prior $\pi(\sigma^2) = \text{Inv.Gamma}(\epsilon, \epsilon)$ with ϵ small (we set it to 10^{-3}), and $\lambda \sim \pi(\lambda) = N_{\lambda>0}(0, 1)$. The SPDE-INLA approach was implemented for $\nu = 0.5$ following Krainski et al. (2019), Chapter 2, setting $\alpha = \nu + 1 = 1.5$. Setting $\nu = 1.5$ was unsupported by `inla.spde2.pcmatern` in R-INLA. The priors on σ^2, ϕ were such that $Pr(\sigma > 2.5) = 0.01$ and $Pr(\phi < 0.1) = 0.01$. The mesh for INLA was fixed

<i>Efficiency</i>		$\nu = 0.5$			$\nu = 1.5$		
		ESS	ESS/s	Relative	ESS	ESS/s	Relative
QMGP -PS	ϕ	270.13	24.89	148.61	142.59	13.15	222.56
	σ^2	242.91	22.39	117.32	219.82	20.27	341.84
	τ^2	101.94	9.36	3.04	618.25	56.96	53.44
QMGP latent	ϕ	3.96	0.28	1.69	3.87	0.28	4.70
	σ^2	4.97	0.36	1.87	5.58	0.40	6.75
	τ^2	149.04	10.67	3.46	215.96	15.48	14.52
NNGP response	ϕ	7.84	0.17	1.00	10.45	0.06	1.00
	σ^2	8.93	0.19	1.00	10.48	0.06	1.00
	τ^2	144.05	3.08	1.00	187.57	1.07	1.00

Table 6: MCMC efficiency in estimating the Matérn parameters in univariate gridded data settings. For posterior samples of size 2500, we report effective sample size—absolute, per unit time, and relative to the NNGP response model.

at a 10000-sized grid which overlapped with the spatial locations of the test set. In other words we used for INLA the same mesh as the reference set in the QMGP-GriPS method. Smaller meshes are associated with faster computations in INLAs but negatively impact predictions and estimation accuracy (especially about the nugget τ^2). All models were run in a Ubuntu 20.04 workstation based on a 12-core, 24-thread AMD Ryzen 9 3900 CPU and 128GB of memory; R version 4.0.3 was linked to Intel MKL 2019.5-075 which includes efficient LAPACK (Anderson et al., 1999) and BLAS (Blackford et al., 2002) libraries for linear algebra. GriPS-based QMGPs were run on 12 threads using OpenMP (Dagum and Menon, 1998), all other models on 22 threads. Figure 8 summarises the compute times for each model, whereas Figure 9 reports all 95% posterior intervals for the estimation of the unknown covariance parameters. Effective sample size reported in the tables throughout the article was calculated using the `effectiveSize` function of R package coda (Plummer et al., 2006).

<i>Estimation</i>		$\nu = 0.5$			$\nu = 1.5$		
		RMSE	M%E	UQ: Covg	RMSE	M%E	UQ: Covg
QMGP -PS	ϕ	1.0655	0.7269	0.8650	1.4607	0.0925	0.7200
	σ^2	1.7736	0.3866	0.8600	1.9217	0.3385	0.8100
	τ^2	0.0047	0.0584	0.7600	0.0017	0.017	0.8550
QMGP latent	ϕ	1.6210	1.0024	0.5750	4.0534	0.3468	0.4700
	σ^2	2.9009	0.6010	0.5700	2.8427	0.7441	0.4550
	τ^2	0.0056	0.0696	0.6850	1.3032	8.0071	0.7400
NNGP response	ϕ	1.3121	1.0352	0.5550	1.7365	0.1765	0.7300
	σ^2	1.8878	0.4124	0.5350	1.5838	0.3094	0.7000
	τ^2	0.0034	0.0424	0.8500	0.0009	0.0137	0.8800

<i>Prediction</i>	$\nu = 0.5$			$\nu = 1.5$		
	RMSPE	CRPS	UQ: Covg	RMSPE	CRPS	UQ: Covg
QMGP-PS	0.3373	0.1886	0.9502	0.2670	0.1461	0.9490
QMGP latent	0.3374	0.1887	0.9506	0.4816	0.2607	0.9554
NNGP response	0.3432	0.1914	0.9778	0.2789	0.1512	0.9782

Table 7: Top: accuracy in estimating the Matérn parameters ϕ, σ^2 plus τ^2 , in univariate settings—root mean square error (*RMSE*), mean absolute percentage error (*M%E*), and uncertainty quantification in terms of coverage (*UQ: Covg*, with target 95%), averaged across 400 datasets. Bottom: accuracy in predictions—root mean square prediction error (*RMSPE*), continuous ranked probability score (*CRPS*), and 95% coverage.

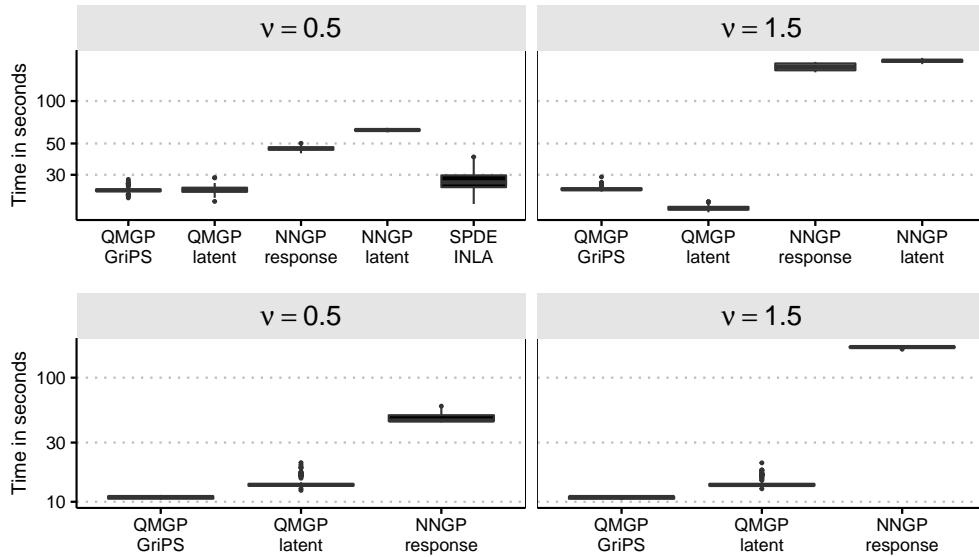


Figure 8: Compute time for each model. The top figure refers to the analysis and models implemented in the main article, the bottom to those in this supplement.

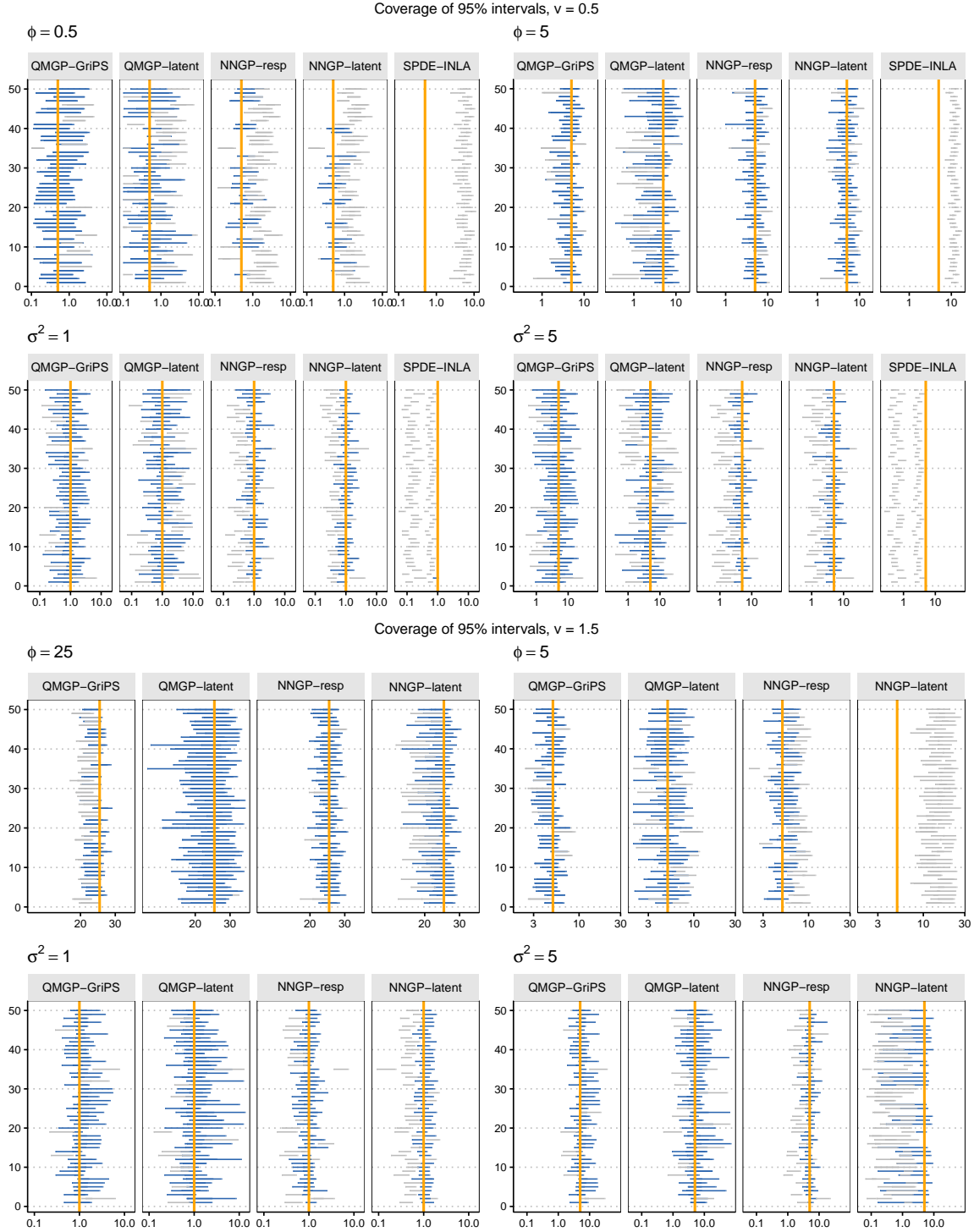


Figure 9: Coverage of posterior 95% intervals in all 400 data sets in the synthetic data application appearing in the main article, and for all models. Orange lines represent the true values; blue lines are 95% (marginal) intervals that include the true value, grey lines are intervals that do not include the true value. Intervals are calculated using MCMC samples of size 2500. SPDE-INLA intervals are extracted from the approximated marginal posterior distributions.

D Additional details on the LiDAR data application

Figures 10 and 11 add to the posterior summaries reported in the main article.

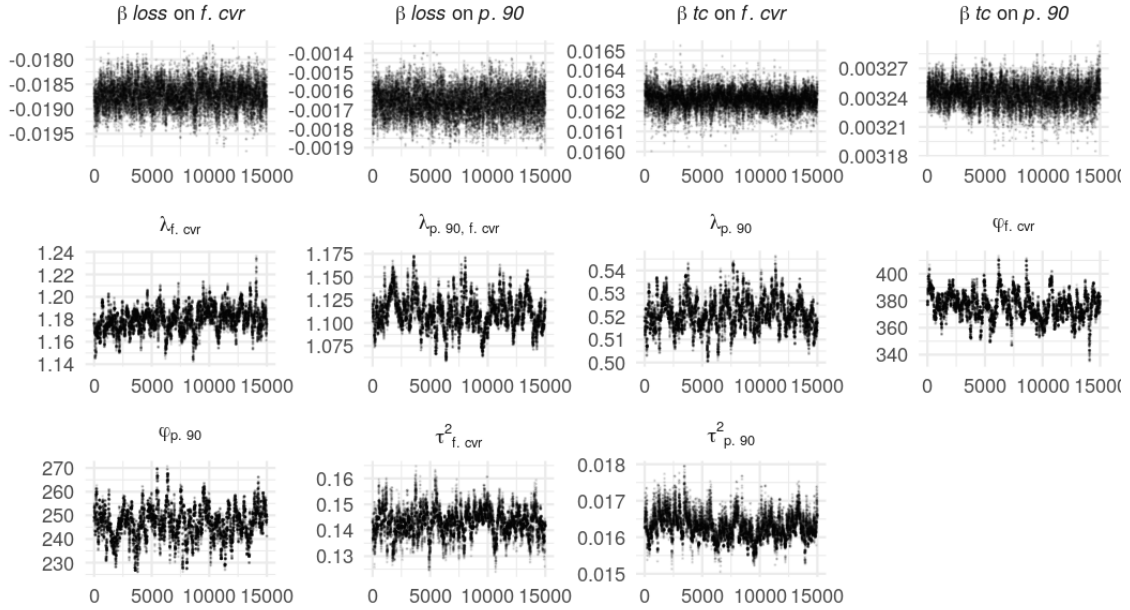


Figure 10: Markov chains for the unknown parameters in the regression model for the LiDAR data.

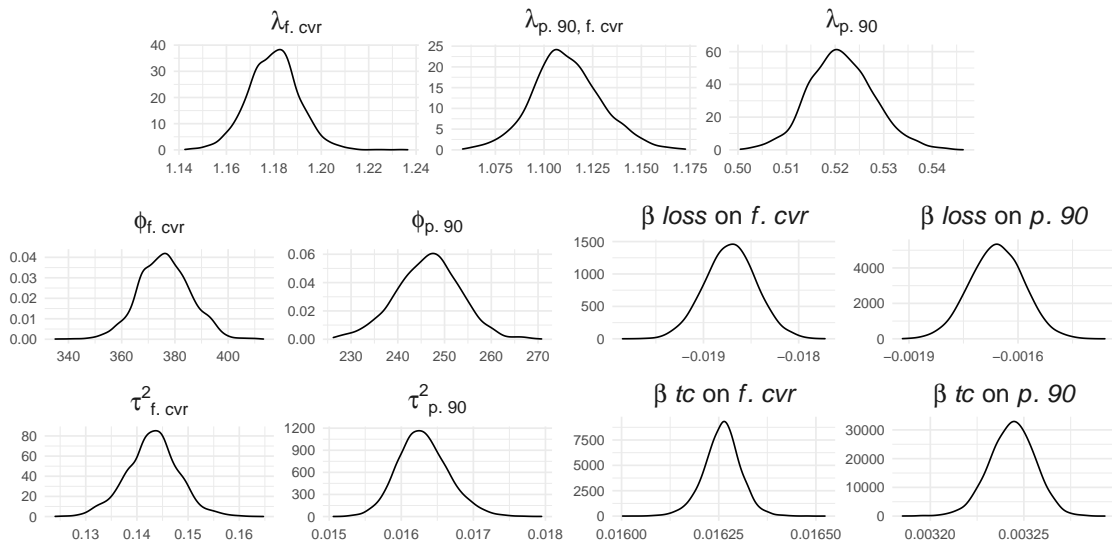


Figure 11: Estimated marginal posterior densities of the covariance parameters $\theta = \{\Lambda, \phi\}$ and regression parameters β and τ^2 .

References

- Ambikasaran, S., Foreman-Mackey, D., Greengard, L., Hogg, D. W., and O’Neil, M. (2016), “Fast Direct Methods for Gaussian Processes,” *IEEE Transactions on Pattern Analysis and Machine Intelligence*, 38, 252–265, doi:10.1109/TPAMI.2015.2448083. 3
- Anderson, E., Bai, Z., Bischof, C., Blackford, S., Demmel, J., Dongarra, J., Du Croz, J., Greenbaum, A., Hammarling, S., McKenney, A., and Sorensen, D. (1999), *LAPACK Users’ Guide*, Philadelphia, PA: Society for Industrial and Applied Mathematics, 3rd ed. 30
- Banerjee, S. (2017), “High-Dimensional Bayesian Geostatistics,” *Bayesian Analysis*, 12, 583–614, doi:10.1214/17-BA1056R. 3, 11
- (2020), “Modeling Massive Spatial Datasets Using a Conjugate Bayesian Linear Modeling Framework,” *Spatial Statistics*, in press, doi:10.1016/j.spasta.2020.100417. 10
- Banerjee, S., Carlin, B. P., and Gelfand, A. E. (2014), *Hierarchical Modeling and Analysis for Spatial Data, 2nd edition*, Chapman and Hall/CRC, doi:10.1201/b17115. 10
- Banerjee, S., Gelfand, A. E., Finley, A. O., and Sang, H. (2008), “Gaussian predictive process models for large spatial data sets,” *Journal of the Royal Statistical Society, Series B*, 70, 825–848, doi:10.1111/j.1467-9868.2008.00663.x. 3, 11, 18
- Blackford, L. S., Petitet, A., Pozo, R., Remington, K., Whaley, R. C., Demmel, J., Dongarra, J., Duff, I., Hammarling, S., Henry, G., et al. (2002), “An updated set of basic linear algebra subprograms (BLAS),” *ACM Transactions on Mathematical Software*, 28, 135–151. 30
- Cook, B. D., Corp, L. A., Nelson, R. F., Middleton, E. M., Morton, D. C., McCorkel, J. T., Masek, J. G., Ranson, K. J., Ly, V., and Montesano, P. M. (2013), “NASA Goddard’s LiDAR, Hyperspectral and Thermal (G-LiHT) Airborne Imager,” *Remote Sensing*, 5, 4045–4066, doi:10.3390/rs5084045. 6, 22
- Cressie, N. and Johannesson, G. (2008), “Fixed Rank Kriging for Very Large Spatial Data Sets,” *Journal of the Royal Statistical Society, Series B*, 70, 209–226, doi:10.1111/j.1467-9868.2007.00633.x. 3
- Dagum, L. and Menon, R. (1998), “OpenMP: an industry standard API for shared-memory programming,” *Computational Science & Engineering, IEEE*, 5, 46–55. 30

- Datta, A., Banerjee, S., Finley, A. O., and Gelfand, A. E. (2016a), “Hierarchical Nearest-Neighbor Gaussian Process Models for Large Geostatistical Datasets,” *Journal of the American Statistical Association*, 111, 800–812, [doi:10.1080/01621459.2015.1044091](https://doi.org/10.1080/01621459.2015.1044091). 3
- Datta, A., Banerjee, S., Finley, A. O., Hamm, N. A. S., and Schaap, M. (2016b), “Nonseparable dynamic nearest neighbor Gaussian process models for large spatio-temporal data with an application to particulate matter analysis,” *The Annals of Applied Statistics*, 10, 1286–1316, [doi:10.1214/16-AOAS931](https://doi.org/10.1214/16-AOAS931). 27
- Dunson, D. and Johndrow, J. E. (2020), “The Hastings algorithm at fifty,” *Biometrika*, 107, 1–23, [doi:10.1093/biomet/asz066](https://doi.org/10.1093/biomet/asz066). 4
- Eidsvik, J., Shaby, B. A., Reich, B. J., Wheeler, M., and Niemi, J. (2014), “Estimation and Prediction in Spatial Models With Block Composite Likelihoods,” *Journal of Computational and Graphical Statistics*, 23, 295–315, [doi:10.1080/10618600.2012.760460](https://doi.org/10.1080/10618600.2012.760460). 3
- Finley, A. O., Banerjee, S., Ek, A. R., and McRoberts, R. E. (2008), “Bayesian multivariate process modeling for prediction of forest attributes,” *Journal of Agricultural, Biological, and Environmental Statistics*, 13, 60, [doi:10.1198/108571108X273160](https://doi.org/10.1198/108571108X273160). 9
- Finley, A. O., Datta, A., Cook, B. D., Morton, D. C., Andersen, H. E., and Banerjee, S. (2019), “Efficient Algorithms for Bayesian Nearest Neighbor Gaussian Processes,” *Journal of Computational and Graphical Statistics*, 28, 401–414, [doi:10.1080/10618600.2018.1537924](https://doi.org/10.1080/10618600.2018.1537924). 5, 11, 23
- Finley, A. O., Sang, H., Banerjee, S., and Gelfand, A. E. (2009), “Improving the performance of predictive process modeling for large datasets,” *Computational Statistics and Data Analysis*, 53, 2873–2884, [doi:10.1016/j.csda.2008.09.008](https://doi.org/10.1016/j.csda.2008.09.008). 15
- Furrer, R., Genton, M. G., and Nychka, D. (2006), “Covariance Tapering for Interpolation of Large Spatial Datasets,” *Journal of Computational and Graphical Statistics*, 15, 502–523, [doi:10.1198/106186006X132178](https://doi.org/10.1198/106186006X132178). 3
- GEDI (2020), “Global Ecosystem Dynamics Investigation LiDAR,” <https://gedi.umd.edu>. 6
- Gelfand, A. E., Sahu, S. K., and Carlin, B. P. (1995), “Efficient Parametrisations for Normal Linear Mixed Models,” *Biometrika*, 82, 479–488, [doi:10.2307/2337527](https://doi.org/10.2307/2337527). 5

- Gelman, A. (2006), “Prior distributions for variance parameters in hierarchical models (comment on article by Browne and Draper),” *Bayesian Analysis*, 1, 513–533, doi:10.1214/06-BA117A. 6, 16
- Genton, M. G. and Kleiber, W. (2015), “Cross-Covariance Functions for Multivariate Geostatistics,” *Statistical Science*, 30, 147–163, doi:10.1214/14-STS487. 7, 27
- Geoga, C. J., Anitescu, M., and Stein, M. L. (2020), “Scalable Gaussian Process Computations Using Hierarchical Matrices,” *Journal of Computational and Graphical Statistics*, 29, 227–237, doi:10.1080/10618600.2019.1652616. 3
- Ghosh, J. and Dunson, D. B. (2009), “Default Prior Distributions and Efficient Posterior Computation in Bayesian Factor Analysis,” *Journal of Computational and Graphical Statistics*, 18, 306–320, doi:10.1198/jcgs.2009.07145. 16
- Gneiting, T., Kleiber, W., and Schlather, M. (2010), “Matérn Cross-Covariance Functions for Multivariate Random Fields,” *Journal of the American Statistical Association*, 105, 1167–1177, doi:10.1198/jasa.2010.tm09420. 27
- Gonzalez, J., Low, Y., Gretton, A., and Guestrin, C. (2011), “Parallel Gibbs Sampling: From Colored Fields to Thin Junction Trees,” in *Proceedings of the Fourteenth International Conference on Artificial Intelligence and Statistics*, eds. Gordon, G., Dunson, D., and Dudík, M., Fort Lauderdale, FL, USA: PMLR, vol. 15 of *Proceedings of Machine Learning Research*, pp. 324–332. 13
- Gramacy, R. B. and Apley, D. W. (2015), “Local Gaussian Process Approximation for Large Computer Experiments,” *Journal of Computational and Graphical Statistics*, 24, 561–578, doi:10.1080/10618600.2014.914442. 3
- Guhaniyogi, R. and Banerjee, S. (2018), “Meta-Kriging: Scalable Bayesian Modeling and Inference for Massive Spatial Datasets,” *Technometrics*, 60, 430–444, doi:10.1080/00401706.2018.1437474. 3
- Guhaniyogi, R., Finley, A. O., Banerjee, S., and Gelfand, A. E. (2011), “Adaptive Gaussian predictive process models for large spatial datasets,” *Environmetrics*, 22, 997–1007, doi:10.1002/env.1131. 12

- Heaton, M. J., Datta, A., Finley, A. O., Furrer, R., Guinness, J., Guhaniyogi, R., Gerber, F., Gramacy, R. B., Hammerling, D., Katzfuss, M., Lindgren, F., Nychka, D. W., Sun, F., and Zammit-Mangion, A. (2019), “A Case Study Competition Among Methods for Analyzing Large Spatial Data,” *Journal of Agricultural, Biological and Environmental Statistics*, 24, 398–425, [doi:10.1007/s13253-018-00348-w](https://doi.org/10.1007/s13253-018-00348-w). 3
- Huang, H. and Sun, Y. (2018), “Hierarchical Low Rank Approximation of Likelihoods for Large Spatial Datasets,” *Journal of Computational and Graphical Statistics*, 27, 110–118, [doi:10.1080/10618600.2017.1356324](https://doi.org/10.1080/10618600.2017.1356324). 3
- ICESat-2 (2020), “Ice, Cloud, and Land Elevation Satellite-2,” <https://icesat-2.gsfc.nasa.gov/>. 6
- Jurek, M. and Katzfuss, M. (2020), “Hierarchical sparse Cholesky decomposition with applications to high-dimensional spatio-temporal filtering,” [arXiv:2006.16901](https://arxiv.org/abs/2006.16901). 3
- Kampe, T. U., Johnson, B. R., Kuester, M. A., and Keller, M. (2010), “NEON: the first continental-scale ecological observatory with airborne remote sensing of vegetation canopy biochemistry and structure,” *Journal of Applied Remote Sensing*, 4, 1–24, [doi:10.1117/1.3361375](https://doi.org/10.1117/1.3361375). 6
- Kastner, Gregor Frühwirth-Schnatter, S. (2014), “Ancillarity-sufficiency interweaving strategy (ASIS) for boosting MCMC estimation of stochastic volatility models,” *Computational Statistics and Data Analysis*, 76, 408–423, [doi:10.1016/j.csda.2013.01.002](https://doi.org/10.1016/j.csda.2013.01.002). 5
- Katzfuss, M. (2017), “A Multi-Resolution Approximation for Massive Spatial Datasets,” *Journal of the American Statistical Association*, 112, 201–214, [doi:10.1080/01621459.2015.1123632](https://doi.org/10.1080/01621459.2015.1123632). 3
- Katzfuss, M. and Guinness, J. (2019), “A general framework for Vecchia approximations of Gaussian processes,” [arXiv:1708.06302](https://arxiv.org/abs/1708.06302). 4, 11
- Kaufman, C. G., Schervish, M. J., and Nychka, D. W. (2008), “Covariance Tapering for Likelihood-Based Estimation in Large Spatial Data Sets,” *Journal of the American Statistical Association*, 103, 1545–1555, [doi:10.1198/016214508000000959](https://doi.org/10.1198/016214508000000959). 3
- Krainski, E. T., Gómez-Rubio, V., Bakka, H., Lenzi, A., Castro-Camilo, D., Simpson, D., Lindgren, F., and Rue, H. (2019), *Advanced Spatial Modeling with Stochastic Partial Differential Equations Using R and INLA*, CRC Press/Taylor and Francis Group. 29

- Krause, A., Singh, A., and Guestrin, C. (2008), “Near-Optimal Sensor Placements in Gaussian Processes: Theory, Efficient Algorithms and Empirical Studies,” *Journal of Machine Learning Research*, 8, 235–284, <http://www.jmlr.org/papers/v9/krause08a.html>. 12
- Lindgren, F., Rue, H., and Lindström, J. (2011), “An explicit link between Gaussian fields and Gaussian Markov random fields: the stochastic partial differential equation approach,” *Journal of the Royal Statistical Society: Series B*, 73, 423–498, doi:10.1111/j.1467-9868.2011.00777.x. 19
- Liu, J. S. and Chen, R. (1995), “Blind Deconvolution via Sequential Imputations,” *Journal of the American Statistical Association*, 90, 567–576, doi:10.1080/01621459.1995.10476549. 8
- Liu, J. S. and Wu, Y. N. (1999), “Parameter Expansion for Data Augmentation,” *Journal of the American Statistical Association*, 94, 1264–1274, doi:10.1080/01621459.1999.10473879. 5
- Matheron, G. (1982), “Pour une analyse krigéante des données régionalisées,” *Technical report N.732, Centre de Géostatistique*. 5
- Papaspiliopoulos, O., O., R. G., and Sköld, M. (2007), “A General Framework for the Parametrization of Hierarchical Models,” *Statistical Science*, 22, 59–73, doi:10.1214/088342307000000014. 5, 9
- Peruzzi, M., Banerjee, S., and Finley, A. O. (2020), “Highly Scalable Bayesian Geostatistical Modeling via Meshed Gaussian Processes on Partitioned Domains,” *Journal of the American Statistical Association*, in press. doi:10.1080/01621459.2020.1833889. 4, 12, 13, 27
- Peruzzi, M. and Dunson, D. B. (2020), “Spatial multivariate trees for big data Bayesian regression,” [arXiv:2012.00943](https://arxiv.org/abs/2012.00943). 4, 11
- Plummer, M., Best, N., Cowles, K., and Vines, K. (2006), “CODA: Convergence Diagnosis and Output Analysis for MCMC,” *R News*, 6, 7–11. 30
- Quiroz, Z. C., Prates, M. O., and Dey, D. K. (2019), “Block Nearest Neighbor Gaussian processes for large datasets,” [arXiv:1604.08403](https://arxiv.org/abs/1604.08403). 4
- Quiñonero-Candela, J. and Rasmussen, C. E. (2005), “A Unifying View of Sparse Approximate Gaussian process Regression,” *Journal of Machine Learning Research*, 6, 1939–1959, <https://www.jmlr.org/papers/volume6/quinonero-candela05a/quinonero-candela05a.pdf>. 3

- Ren, Q. and Banerjee, S. (2013), “Hierarchical Factor Models for Large Spatially Misaligned Data: A Low-Rank Predictive Process Approach,” *Biometrics*, 69, 19–30, [doi:10.1111/j.1541-0420.2012.01832.x](https://doi.org/10.1111/j.1541-0420.2012.01832.x). 10
- Robert, C. P. and Casella, G. (2005), *Monte Carlo Statistical Methods (Springer Texts in Statistics)*, Berlin, Heidelberg: Springer-Verlag. 4, 8
- Rue, H. and Held, L. (2005), *Gaussian Markov Random Fields: Theory and Applications*, Chapman & Hall/CRC, [doi:10.1007/978-3-642-20192-9](https://doi.org/10.1007/978-3-642-20192-9). 3
- Rue, H., Martino, S., and Chopin, N. (2009), “Approximate Bayesian inference for latent Gaussian models by using integrated nested Laplace approximations,” *Journal of the Royal Statistical Society: Series B*, 71, 319–392, [doi:10.1111/j.1467-9868.2008.00700.x](https://doi.org/10.1111/j.1467-9868.2008.00700.x). 19
- Sang, H. and Huang, J. Z. (2012), “A full scale approximation of covariance functions for large spatial data sets,” *Journal of the Royal Statistical Society, Series B*, 74, 111–132, [doi:10.1111/j.1467-9868.2011.01007.x](https://doi.org/10.1111/j.1467-9868.2011.01007.x). 3
- Shirota, S., Finley, A. O., Cook, B. D., and Banerjee, S. (2019), “Conjugate Nearest Neighbor Gaussian Process Models for Efficient Statistical Interpolation of Large Spatial Data,” [arXiv:1907.10109](https://arxiv.org/abs/1907.10109). 10
- Snelson, E. and Ghahramani, Z. (2007), “Local and global sparse Gaussian process approximations,” in *Proceedings of the Eleventh International Conference on Artificial Intelligence and Statistics*, vol. 2 of *Proceedings of Machine Learning Research*, pp. 524–531, <http://proceedings.mlr.press/v2/snelson07a.html>. 3
- Stein, M. (1990), “Uniform Asymptotic Optimality of Linear Predictions of a Random Field Using an Incorrect Second-Order Structure,” *The Annals of Statistics*, 18, 850–872, [doi:10.1214/aos/1176347629](https://doi.org/10.1214/aos/1176347629). 5, 10
- Stein, M. L. (1999), *Interpolation of spatial data: Some theory for Kriging*, Springer Series in Statistics, New York: Springer-Verlag, [doi:10.1007/978-1-4612-1494-6](https://doi.org/10.1007/978-1-4612-1494-6). 6, 15
- (2014), “Limitations on low rank approximations for covariance matrices of spatial data,” *Spatial Statistics*, 8, 1–19, [doi:doi:10.1016/j.spasta.2013.06.003](https://doi.org/10.1016/j.spasta.2013.06.003). 3

- Sun, Y., Li, B., and Genton, M. (2011), “Geostatistics for large datasets,” in *Advances and Challenges in Space-time Modelling of Natural Events*, eds. Montero, J., Porcu, E., and Schlather, M., Berlin Heidelberg: Springer-Verlag, pp. 55–77, [doi:10.1007/978-3-642-17086-7](https://doi.org/10.1007/978-3-642-17086-7). 3
- Tang, W., Zhang, L., and Banerjee, S. (2020), “On identifiability and consistency of the nugget in Gaussian spatial process models,” [arXiv:1908.05726](https://arxiv.org/abs/1908.05726). 5, 10
- Taylor-Rodriguez, D., Finley, A. O., Datta, A., Babcock, C., Andersen, H. E., Cook, B. D., Morton, D. C., and Banerjee, S. (2019), “Spatial factor models for high-dimensional and large spatial data: An application in forest variable mapping,” *Statistica Sinica*, 29, 1155–1180, [doi:10.5705/ss.202018.0005](https://doi.org/10.5705/ss.202018.0005). 10
- van Dyk, D. A. and Meng, X.-L. (2001), “The Art of Data Augmentation,” *Journal of Computational and Graphical Statistics*, 10, 1–50, [doi:10.1198/10618600152418584](https://doi.org/10.1198/10618600152418584). 5
- Vecchia, A. V. (1988), “Estimation and Model Identification for Continuous Spatial Processes,” *Journal of the Royal Statistical Society, Series B*, 50, 297–312, [doi:10.1111/j.2517-6161.1988.tb01729.x](https://doi.org/10.1111/j.2517-6161.1988.tb01729.x). 3
- Vihola, M. (2012), “Robust adaptive Metropolis algorithm with coerced acceptance rate,” *Statistics and Computing*, 22, 997–1008, [doi:10.1007/s11222-011-9269-5](https://doi.org/10.1007/s11222-011-9269-5). 18
- Wackernagel, H. (2003), *Multivariate Geostatistics: An Introduction with Applications*, Springer, Berlin, [doi:10.1007/978-3-662-05294-5](https://doi.org/10.1007/978-3-662-05294-5). 5
- Ying, Z. (1991), “Asymptotic properties of a maximum likelihood estimator with data from a Gaussian process,” *Journal of Multivariate Analysis*, 36, 280–296, [doi:10.1016/0047-259X\(91\)90062-7](https://doi.org/10.1016/0047-259X(91)90062-7). 5, 10
- Yu, Y. and Meng, X.-L. (2011), “To Center or Not to Center: That Is Not the Question—An Ancillarity–Sufficiency Interweaving Strategy (ASIS) for Boosting MCMC Efficiency,” *Journal of Computational and Graphical Statistics*, 20, 531–570, [doi:10.1198/jcgs.2011.203main](https://doi.org/10.1198/jcgs.2011.203main). 5
- Zhang, H. (2004), “Inconsistent Estimation and Asymptotically Equal Interpolations in Model-Based Geostatistics,” *Journal of the American Statistical Association*, 99, 250–261, [doi:10.1198/016214504000000241](https://doi.org/10.1198/016214504000000241). 5, 10
- Zhang, L. and Banerjee, S. (2020), “Spatial Factor Modeling: A Bayesian Matrix-Normal Approach for Misaligned Data,” [arXiv:2006.00595](https://arxiv.org/abs/2006.00595). 5, 9, 10, 27